Journal Pre-proof

Global Functional Genomics Reveals GRK5 as a Cystic Fibrosis Therapeutic Target Synergistic with Current Modulators

Hugo M. Botelho, Miquéias Lopes-Pacheco, Madalena C. Pinto, Violeta Railean, Ines Pankonien, Mariana F. Caleiro, Luka A. Clarke, Vasco Cachatra, Beate Neumann, Christian Tischer, Cristina Moiteiro, Jiraporn Ousingsawat, Karl Kunzelmann, Rainer Pepperkok, Margarida D. Amaral

PII: S2589-0042(25)00202-0

DOI: https://doi.org/10.1016/j.isci.2025.111942

Reference: ISCI 111942

To appear in: *ISCIENCE*

Received Date: 19 August 2022

Revised Date: 2 December 2024

Accepted Date: 13 January 2025

Please cite this article as: Botelho, H.M., Lopes-Pacheco, M., Pinto, M.C., Railean, V., Pankonien, I., Caleiro, M.F., Clarke, L.A., Cachatra, V., Neumann, B., Tischer, C., Moiteiro, C., Ousingsawat, J., Kunzelmann, K., Pepperkok, R., Amaral, M.D., Global Functional Genomics Reveals GRK5 as a Cystic Fibrosis Therapeutic Target Synergistic with Current Modulators, *ISCIENCE* (2025), doi: https://doi.org/10.1016/j.isci.2025.111942.

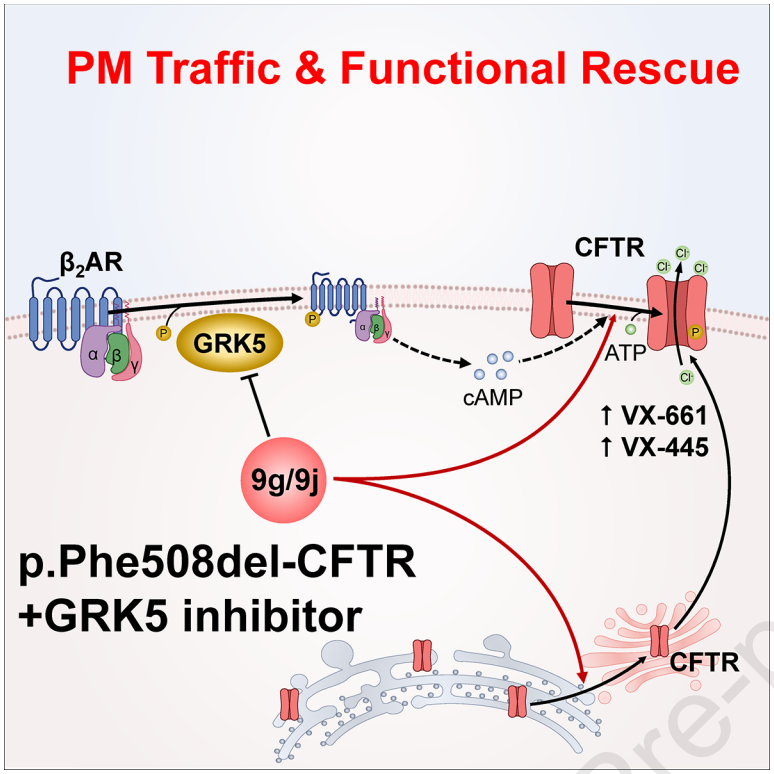

Global Functional Genomics Reveals GRK5 as a Cystic Fibrosis Therapeutic Target Synergistic with Current Modulators

Hugo M. Botelho[1], Miquéias Lopes-Pacheco[1], Madalena C. Pinto[1,2], Violeta Railean[1], Ines Pankonien[1], Mariana F. Caleiro[1], Luka A. Clarke[1], Vasco Cachatra[3], Beate Neumann[4], Christian Tischer[4,5], Cristina Moiteiro[3], Jiraporn Ousingsawat[2], Karl Kunzelmann[2], Rainer Pepperkok[4], Margarida D. Amaral[1]*

[1]BioISI – Biosystems & Integrative Sciences Institute, Faculty of Sciences, University of Lisboa. Campo Grande, 1749-016 Lisboa, Portugal

[2]Department of Physiology, University of Regensburg. Universitätsstrasse 31, 93053 Regensburg, Germany

[3]Centro de Química Estrutural, Institute of Molecular Sciences, Department of Chemistry and Biochemistry, Faculty of Sciences, University of Lisboa. Campo Grande, 1749-016 Lisboa, Portugal

[4]Cell Biology and Biophysics Unit and Advanced Light Microscopy Facility. European Molecular Biology Laboratory (EMBL). Meyerhofstraße 1, 69117 Heidelberg, Germany

[5]Centre for Bioimage Analysis. European Molecular Biology Laboratory (EMBL). Meyerhofstraße 1, 69117 Heidelberg, Germany

* Lead contact:

Margarida D. Amaral

Email: mdamaral@ciencias.ulisboa.pt

Tel: +351 21 750 0861

Fax: +351 21 750 0088

Summary

Cystic Fibrosis (CF) is a life-shortening disease affecting >160,000 individuals worldwide predominantly with respiratory symptoms. About 80% of individuals with CF have the p.Phe508del variant that causes the CF transmembrane conductance regulator (CFTR) protein to misfold and be targeted for premature degradation by the endoplasmic reticulum (ER) quality control (ERQC), thus preventing its plasma membrane (PM) traffic. Despite the recent approval of a 'highly effective' drug rescuing p.Phe508del-CFTR, maximal lung function improvement is ~14%. To identify global modulators of p.Phe508del traffic, we performed a high-content siRNA microscopy-based screen of >9,000 genes and monitored p.Phe508del-CFTR PM rescue in human airway cells. This primary screen identified 227 p.Phe508del-CFTR traffic regulators, of which 35 could be validated by additional siRNAs. Subsequent mechanistic studies established GRK5 as a robust regulator whose inhibition rescues p.Phe508del-CFTR PM traffic and function in primary and immortalized cells, thus emerging as a novel potential drug target for CF.

Keywords: endoplasmic reticulum; quality control; protein folding; traffic disorders; high-content screening; siRNA; high-throughput microscopy; drug discovery; secretory traffic; GRK5

Abbreviations:

ABC, ATP binding cassette (transporter); AFT, arginine-framed tripeptide; ASL, airway surface liquid; CF, Cystic Fibrosis; CFTR, CF Transmembrane Conductance Regulator; COPII, coat protein II (coated vesicles); DIPEA, N,N-diisopropylethylamine; DMTMM, 4-(4,6-dimethoxy-1,3,5-triazin-2-yl)-4-methyl-morpholinium chloride; DMF, N-N-dimethylformamide; ER, endoplasmic reticulum; ERQC, ER quality control; Fsk, forskolin; HATU, 1-[Bis(imethylamino)methylene]-1H-1,2,3-triazolo[4,5,b]pyridinium-3-oxide hexafluorophosphate; HS-YFP, halide-sensitive yellow fluorescence protein; HT, high-throughput; HCS high-content screening; ICL4, intracellular loop 4; MSD1, membrane spanning domain 1; NBD1(2) nucleotide-binding domain 1(2); pHBE, primary human bronchial epithelial (cells); PM, plasma membrane; RD, regulatory domain; UPP, Ub-proteasomal pathway; WB, Western blot(ting).

Introduction

Mutations in the gene encoding the Cystic Fibrosis Transmembrane Conductance Regulator (CFTR) protein [1] cause Cystic Fibrosis (CF), the most common life-shortening autosomal recessive disease (median age at death ~37 years [2]) affecting >160,000 individuals worldwide[3]. CFTR is a chloride (Cl^-) and bicarbonate (HCO_3^-) channel expressed at the apical membrane of several epithelial tissues, notably the airways, which constitute the most affected organ in CF. In the airways, CFTR maintains epithelial ion homeostasis, fluid secretion and hydration of the airway surface liquid (ASL). Dysfunctional CFTR leads to ASL dehydration and persistence of a thick mucus which obstructs the airway and prevents mucociliary clearance. This potentiates chronic inflammation and recurrent bacterial infections that lead to progressive deterioration of lung function, the most frequent cause of morbidity and mortality in CF.

Among the >2,100 CFTR variants so far reported [4], the most common one is deletion of residue phenylalanine 508 – p.Phe508del (legacy name: F508del-CFTR) – which occurs in ~80% of CF cases, thus being a preferential target for research and drug development. p.Phe508del-CFTR presents several defects, namely: *i)* **protein misfolding** which is resistant to physiological rescue by endogenous molecular chaperones; *ii)* **deficient PM traffic** due to retention of misfolded p.Phe508del-CFTR at several checkpoints of the ER quality control (ERQC) machinery [5] which target it for premature degradation via the ubiquitin-proteasome pathway (UPP); *iii)* **impaired function**, as the residual amount of p.Phe508del-CFTR that reaches the PM (only in some individuals) has very low activity due to a channel gating defect [6]; *iv)* **PM instability** of rescued p.Phe508del-CFTR as it is quickly endocytosed and degraded [7,8].

Early studies have shown that p.Phe508del-CFTR can be released from the ER to the PM, namely by low temperature expression [9]. Nevertheless, only recently a highly effective triple combination drug comprising two correctors – tezacaftor (VX-661) and elexacaftor (VX-445), to rescue p.Phe508del-CFTR PM traffic – with a potentiator – ivacaftor (VX-770), to rescue the gating defect – was shown to be efficacious in CF individuals bearing one or two p.Phe508del alleles [10,11]. Even so, the maximum clinical benefit of this highly effective drug is estimated at an average ~14% lung function improvement ($ppFEV_1$), with some individuals with less than 5% $ppFEV_1$ increase.

Evidence supports the binding of tezacaftor and the first generation corrector lumacaftor (VX-809) to CFTR [8,12,13] where they restore the interaction between the first nucleotide binding domain (NBD1) and the fourth intracellular loop (ICL4) [14]. However, the mechanism of action (MoA) for the elexacaftor corrector remains elusive. Modelling studies have suggested binding to the same lumacaftor/tezacaftor site and/or to a distinct site at the first membrane spanning domain (MSD1) [15]. The identification of the machinery assessing CFTR folding at ERQC checkpoints [16,17] will likely shed light on the MoA of this and future traffic-rescuing drugs [18]. Likewise, global knowledge on ERQC intervenients is expected to contribute towards the rational development of improved therapeutic strategies aimed at rescuing p.Phe508del-CFTR, as well as other CFTR folding variants, and/or other misfolded proteins causing traffic disorders [19].

The complex ERQC process by which CFTR folding is assessed has been proposed to consist of at least four sequential checkpoints [16,20,21], namely through: 1) interaction with the Hsp70 chaperone machinery where

most p.Phe508del-CFTR is degraded; 2) the calnexin folding cycle; 3) exposure to an unidentified machinery retaining arginine-framed tripeptides (AFT: Arg-X-Arg), four of which are present in CFTR; and 4) interaction of the CFTR di-acidic exit code (Asp^{565}-Ala-Asp^{567}) with Sec23/Sec24 for ER exit through coat protein (COP) II-coated vesicles [22,23]. Failure to overcome one or more checkpoints inevitably leads to CFTR retention in the ER and subsequent degradation via UPP. Most of the knowledge on the ERQC checkpoints was obtained through studies with second-site "revertant" variants which render p.Phe508del-CFTR less susceptible to UPP at selected checkpoints [17,24,25]. Revertants also enabled dissection of the MoA of corrector drugs [14]. The factors that retain p.Phe508del-CFTR at each ERQC checkpoint have been elucidated by hypothesis-driven approaches, being thus likely that many remain unidentified.

Here, we hypothesized the existence of still unidentified cellular factors retaining p.Phe508del-CFTR in the ER which might become potential drug targets for CF as well as for other diseases caused by misfolded proteins. To identify these factors on a global scale, we applied a cell-based high-throughput (HT) microscopy approach using loss of function assays to screen a druggable genome library comprising 27,310 siRNAs for PM rescue of p.Phe508del-CFTR [26,27]. After carrying out hit validation, mechanistic classification according to ERQC checkpoint targets and assessment of CFTR rescue additivity with state-of-the art folding corrector drugs, we eventually selected five kinase proteins and studied their MoA. Of these, G Protein-Coupled Receptor Kinase 5 (GRK5) was selected as the hit with highest druggable potential, based on the rescue of p.Phe508del-CFTR traffic and function upon its inhibition by either siRNAs or recently reported selective inhibitors – 9g or 9j – in a manner additive to CFTR correctors. We thus propose GRK5 as a potential therapeutic target for CF and discuss the mechanism by which GRK5 inhibition may rescue p.Phe508del-CFTR from its ER retention.

Results

Primary screen to identify global regulators of p.Phe508del-CFTR traffic

To identify genes retaining p.Phe508del-CFTR in the ER we deployed an established high-content screening (HCS) pipeline based on a Tet-inducible p.Phe508del-CFTR traffic reporter (mCherry-Flag-p.Phe508del-CFTR) stably expressed in human airway cells [26]. This pipeline was used to screen the Ambion Human Extended Druggable Genome siRNA library (27,310 siRNAs targeting 9,126 genes, **Fig.1A, Dataset S1A**). Our main readout was the amount of p.Phe508del-CFTR at the PM since KD of p.Phe508del-CFTR ER retention factors are expected to increase the amount of this variant at the cell surface and, consequently, channel activity. Data was expressed as a Z-score which took the 5×5 neighbouring wells as baseline (Z-score5×5, **Fig. S1**). After filtering out siRNAs with multiple or non-protein coding targets, plates with unsuccessful siRNA coating and non-representative cells 21,843 siRNAs, targeting 8,592 genes, were scored regarding p.Phe508del-CFTR PM levels. Targeted genes were classified as positive or negative hits, whenever their siRNA KD resulted in significant enhancement ($Z\text{-score}_{5\times5} \geq +2$) or reduction/inhibition ($Z\text{-score}_{5\times5} \leq -2$) of PM p.Phe508del-CFTR, respectively. Positive gene hits are the putative p.Phe508del-CFTR retention factors of interest. Using this

stringent criterion, we identified 227 genes, targeted by 228 siRNAs, as positive hits (**Fig.1B,C**, **Dataset S1B**). Only 1 gene had 2 distinct siRNAs leading to p.Phe508del-CFTR PM rescue, UQCRFS1 (ubiquinol-cytochrome c reductase, Rieske iron-sulphur polypeptide 1). Conversely, we could still identify 91 genes, targeted by 92 siRNAs, as negative hits (**Dataset S1C**). In the primary screen p.Phe508del-CFTR PM levels were highly correlated (Spearman's $\rho = 0.93$, $p < 2.2x10^{-16}$) with CFTR traffic efficiency (the Flag/mCherry fluorescence ratio), which was also computed.

To gain insight into the nature of primary hits, we performed overrepresentation tests on the Gene Ontology (GO) terms associated with these genes, including positive (**Fig.S2A-C**, **Dataset S2A-C**) and negative hits (**Fig.S2D-F**, **Dataset S2CD-F**). In the positive hit genes, we found overrepresentation of the terms PM (cell component), kinase activity, ionic binding and transport and adenylyl nucleotide binding (molecular function) and phosphorylation (biological process). These terms suggested that several positive hits are other PM proteins, possibly competing with CFTR to access the secretory pathway through the ERQC machinery. Regarding negative hits, GO revealed an enrichment in PM proteins (cellular component), enzymes and metal binding, pointing to biological pathways possibly favouring p.Phe508del-CFTR traffic.

Secondary screen to confirm primary screen hits as retention factors of p.Phe508del-CFTR traffic

Primary screen hits were rescreened using distinct siRNA molecules. A secondary library of 450 siRNAs targeting 225 of the 227 positive hit genes was assembled (siRNAs were unavailable for two genes) and p.Phe508del-CFTR PM levels were scored by the same traffic assay (**Fig.2A**). In this assay we considered negative hits when Z-score ≤ -1 and positive his when Z-score ≥ +1. We could confirm 35 genes, each targeted by 2 distinct siRNAs, whose KD robustly increased p.Phe508del-CFTR PM levels in both the primary and secondary screening rounds (**Table S1**, **Dataset S3**). This stringent criterion equates to a 15% hit validation rate. When inhibited, these "confirmed gene hits" robustly increased p.Phe508del-CFTR PM availability (**Fig.2B,C**), further supporting their role as p.Phe508del-CFTR retention factors. Notably, in both screening rounds the confirmed hits rescued p.Phe508del-CFTR to a larger extent than the clinical drug VX-809 (lumacaftor, 3 µM). Enrichment analysis of these 35 hit genes did not reveal any overrepresentation of GO terms, likely due to the small sample size.

Validation of p.Phe508del-CFTR traffic regulators by processing and functional assessment

Since the 35 confirmed hits were defined solely by the microscopy-based assay, we performed complementary experiments to further validate them as p.Phe508del-CFTR regulators. CFTR is a glycoprotein which, with an ER-specific core glycosylated form observable in WB as a "band B". ER exit is followed by processing in the Golgi apparatus to yield a high molecular weight fully-glycosylated form, "band C". Through densitometric analysis, the fraction of processed CFTR can be determined as [C/(B+C)]. We transfected CFBE cells expressing untagged p.Phe508del-CFTR with siRNAs targeting each of the 35 confirmed hits, performed WB and

investigated KDs which increased band C over the control (**Fig.3, Table S2**). These experiments validated 32 of the 35 genes (91%) as putative regulators of p.Phe508del-CFTR PM traffic (statistically significant band C increases over control for at least 1 siRNA). Of these, 17 siRNAs also increased processing (ARVCF, CCL27, COL5A1, DCSTAMP, GJB2, IL24, ISL2, KIF17, LRRK1, NTNG2, PCDHB2, RECQL5, SLC30A1, STYK1, TPK1, VSP26A, ZNF384). This remarkable validation rate, together with the above stringent hit selection criterion, prompted us to examine whether the genes targeted by siRNAs which scored just below the hit threshold in the secondary HCS could also significantly rescue p.Phe508del-CFTR processing. Therefore, WB analysis after knocking-down 18 additional gene hits recovered from the primary screen, but which were not confirmed in the secondary screen, showed for all a significant band C increase versus the control (**Fig.S3, Table S2**). Interestingly, among the 50 genes validated in the WB assay, five kinases yielded some of the highest band C readouts: LRRK1, TPK1, STYK1, GRK5 and DGKG. The LRRK1, TPK1 and STYK1 KDs produced p.Phe508del-CFTR rescue in both HCS rounds and WB assays. To determine the physiological relevance of all 53 genes analysed through HCS and/or WB, we assessed their expression in human native lung tissue by RT-PCR as well as in wt-CFTR expressing CFBE cells (**Dataset S4**). All but 4 genes (CITED2, KIF17, ACSBG2, GUCY2D) were expressed in human native lung tissue (92.4%). Expression of 3 genes (APOB, ACSBG2, GUCY2D) could not be detected in CFBE cells. Of relevance, the 18 genes confirmed exclusively by WB were expressed in both specimens.
To determine whether the 53 confirmed hit genes (considering HCS and WB) also rescue p.Phe508del-CFTR Cl^- conductance, we performed the halide-sensitive YFP (HS-YFP) fluorescence quenching assay after siRNA KDs as in the secondary screen (**Fig. 4**, **Dataset S5**). Cells expressing wt-CFTR were also tested. The assay validated 20 of the 35 HCS confirmed hit genes targeted by 26 siRNAs, whose KD significantly enhanced p.Phe508del-CFTR function above control (Z-score > +1), including LRRK1 and STYK1, but not TPK1. Regarding the 18 additional genes, 13 of them were tested, and KD of 7 genes by 9 siRNAs enhanced p.Phe508del-CFTR function. Overall, KD of 12 of these 27 genes enhanced p.Phe508del- but not wt-CFTR function: CITED2, CLDN4, COL5A1, CREBBP, DCSTAMP, EPN3, FER, FOLR2, KIF17, LDLRAD3, PCDHB2, RECQL5 and ZNF384 (**Dataset S5G**). Conversely, only 2 gene KDs enhanced wt- but not p.Phe508del-CFTR function: QRSL1 and TPK1.

Classification of traffic regulators regarding ERQC checkpoints and CFTR global datasets

We hypothesized that some of the p.Phe508del-CFTR traffic hits could be constituents of the ERQC checkpoints. To test this hypothesis, we assessed the effects of their KD on the traffic of: *i)* wt-CFTR; *ii)*, p.Phe508del-CFTR revertant variants (p.Phe508del-p.Gly550Glu-CFTR [legacy: F508del-G550E-CFTR], p.Phe508del-p.Arg1070Trp-CFTR [legacy: F508del-R1070W-CFTR], p.Phe508del-4RK-CFTR); or *iii)* a traffic-inhibiting CFTR variant (DD/AA-CFTR), all stably expressed in CFBE cell lines as double-tagged (mCherry/Flag) Tet-inducible traffic reporters. This “classification screen” aimed at assigning each hit gene to one or more ERQC checkpoints (**Fig.1A**). These 5 cell lines were reverse transfected with the 450 siRNA secondary library and a positive effect was considered when at least 1 siRNA significantly increased CFTR PM levels (Z-score > +1, **Dataset S6**). Treatment with VX-809 was used in parallel as a positive control. When excluding control siRNAs we obtained a positive effect for 22 genes for wt-CFTR, 52 genes for p.Phe508del-p.Gly550Glu-CFTR, 20 genes

for p.Phe508del-p.Arg1070Trp-CFTR, 25 genes for p.Phe508del-4RK-CFTR and 38 genes for DD/AA-CFTR (**Dataset S6**). To ascertain specificity, we searched for gene KDs which enhanced CFTR PM delivery in wt-, p.Phe508del revertants and DD/AA-CFTR, but not in p.Phe508del-CFTR. We identified such an effect in 13 genes for wt-CFTR, 40 genes for p.Phe508del-p.Gly550Glu-CFTR, 14 genes for p.Phe508del-p.Arg1070Trp-CFTR, 22 genes for p.Phe508del-4RK-CFTR and 32 genes for DD/AA-CFTR (**Table S3**). Conversely, to ascertain ERQC involvement, we searched for gene KDs which had opposite effects on PM delivery of p.Phe508del-CFTR (enhancers) and other variants (inhibitors). We identified such an effect on 19 genes for wt-CFTR, 5 genes for p.Phe508del-p.Gly550Glu-CFTR, 14 genes for p.Phe508del-p.Arg1070Trp-CFTR, 9 genes for p.Phe508del-4RK-CFTR and 4 genes for DD/AA-CFTR (**Table S4**). This last set of genes represented candidate p.Phe508del-CFTR ER retention factors which act at the ERQC checkpoints modulated by these CFTR variants.

To obtain additional information on the specificity and MoA of the 53 confirmed hit genes we performed hierarchical clustering of the classification screen data (**Fig.S4A**). We considered all hit siRNAs and identified 5 clusters, where gene KD produced the following general phenotypes: Cluster 1) strong inhibition of wt-, p.Phe508del-p.Arg1070Trp- and p.Phe508del-4RK-CFTR traffic, with enhancement of p.Phe508del-CFTR traffic with or without VX-809; Cluster 2) strong enhancement of p.Phe508del- regardless of VX-809, p.Phe508del-p.Gly550Glu- and DD/AA-CFTR, and mixed effects on other CFTR variants; Cluster 3) moderate enhancement of all variants; Cluster 4) preferential enhancement of p.Phe508del-CFTR regardless of VX-809, with moderate effect on other variants; Cluster 5) preferential enhancement of p.Phe508del-CFTR, sometimes maximized by VX-809 or the p.Gly550Glu revertant, with moderate or inhibitory effects on other variants.

This classification suggested that genes in Clusters 1 and 2 are highly specific as p.Phe508del-CFTR traffic regulators, while those in the remaining clusters seem less specific, given the overall milder or antagonistic KD phenotype on other CFTR variants. Cluster 3 gathers general CFTR ER retention factors, unrelated to ERQC checkpoints, given the mostly enhanced traffic readout on all variants. The rescue of p.Phe508del-CFTR PM localization by siRNAs targeting Cluster 5 genes seems to be additive with NBD1 folding, given the enhanced rescue when combined with either VX-809 (e.g. siGJB2) or p.Gly550Glu (e.g. siEVI5L, siLRRK1), a revertant proposed to stabilize NBD1 conformation and dimerization. Involvement in ERQC checkpoints is further suggested by the inhibitory effect of most cluster 5 gene KDs in wt-CFTR traffic. Interpretation of the contribution of most genes is not clear, possibly due to genes targeting more than one checkpoint or non-ERQC pathways (**Fig. S4B**). Nevertheless, the kinases in this gene set (LRRK1, TPK1 and STYK1) seem to be specific p.Phe508del-CFTR regulators, given that rescue is not maximized when accessing non-p.Phe508del-CFTR variants, with the notable exception of LRRK1 in p.Phe508del-p.Gly550Glu-CFTR (**Fig. S4C**).

To ascertain the overall pathways targeted by the p.Phe508del-CFTR traffic regulators identified here, we compared the primary and secondary screen hits (including the 53 genes validated by HCS or WB) with published datasets of global CFTR interactors and CF disease modulators (**Fig.S4D**), namely: p.Phe508del-CFTR interactome in HBE41o$^-$ cells [28]; p.Phe508del-CFTR interactome in CFBE41o$^-$ cells [29,30]; genes whose silencing significantly rescued p.Phe508del-CFTR channel activity [31]; candidate modifier genes of CF lung disease [32]; ENaC activating genes in A549 cells [33]; and protein secretion machinery in HeLa cells [34]. Partial interactomes (*e.g.* PM-CFTR only [35]) were not included in this analysis so as to widen the scope as much as possible. We

found 221 instances where the same gene was mentioned in pairs of published datasets. When inspecting our primary and secondary screen hits, there were 32 instances where these hits were mentioned in other studies. Amongst the 53 hits, only 8 appear in other datasets: ARVF and NRIP1 (Dang *et al*), COL5A1 and MYH14 (Reilly *et al*) and CNR2, FER, GOSR2 and OXSR1 (Simpson *et al*). When considering the 5 kinases mentioned above, only GRK5 was found in another dataset (Almaça *et al*), indicating that knocking down GRK5 may not only recue p.Phe508del-CFTR traffic but also inhibit ENaC activity. The low number of genes common to this study and the dataset selection suggests that our HCS platform is sensitive to identify CFTR regulators which may not directly interact with CFTR or may be still unidentified elements of CFTR regulatory networks.

Selection of 5 kinases as top hits of high druggability potential

Since we aimed to identify druggable targets enhancing p.Phe508del-CFTR PM localization, we focused on kinase genes, given their amenability to small-molecule inhibition which makes them preferential drug targets. Thus, among the hit genes identified 5 kinases were selected for further studies: LRRK1, TPK1, STYK1, GRK5 and DGKG (**Fig.1A**). LRRK1, TPK1 and STYK1 were hits in the primary and secondary HCS, as well on the WB validation. GRK5 and DGKG were hits with high PM scores in the primary screen (4.6 and 3.4, respectively, **Dataset S1B**) and with a robust p.Phe508del-CFTR rescue on WB (18- and 12.3-fold change in band C, respectively, **Table S2**). To determine whether these kinases act through the same MoA as CFTR corrector drugs, we performed KD of each kinase in CFBE cells expressing non-tagged p.Phe508del-CFTR with and without combined administration of VX-809 (3 μM) and VX-661 (5 μM) (**Fig.5**). Band C rescue was additive with correctors for GRK5 and LRRK1, and unaffected by DGKG or STYK1 KD. TPK1 KD reduced band C levels in the presence of correctors.

To further examine the pharmacological relevance of the 5 kinases, we assessed the effects of their down-regulation in whole-cell patch-clamp experiments. Control experiments showed the characteristic outwardly rectifying current of wt-CFTR [36-39](**Fig. S5**). The KD of 4 kinases (STYK1, TPK1, GRK5 and LRRK1) significantly rescued p.Phe508del-CFTR function, with GRK5 and STYK1 being the most effective, and DGKG having no effect (**Fig.6**). The presence of VX-809 was additive to either GRK5 or LRRK1 KD.

To more clearly describe the participation of hit kinases on ERQC checkpoints, we examined the combined effect of siRNA KD on the rescue of p.Phe508del-CFTR revertants (p.Phe508del-p.Gly550Glu, p.Phe508del-p.Arg1070Trp, p.Phe508del-4RK) or the DD/AA-CFTR traffic variant (**Fig.S6**). Kinase KDs produced a complex response in the p.Phe508del-p.Gly550Glu and p.Phe508del-p.Arg1070Trp revertants, which target the first ERQC checkpoint. Knocking down LRRK1 or STYK1 did not significantly affect band C levels in most situations, either alone or in the presence of correctors, indicating that these KDs may act at the level of this folding checkpoint. However, STYK1 KD was additive to corrector treatment of p.Phe508del-p.Arg1070Trp-CFTR, suggesting targeting of the ICL4/NBD1 interface [8,40]. DGKG KD was additive to VX-661 but the effect was lost in the presence of VX-445. TPK1 and DGKG KD were mostly additive to VX-661. Rescue by GRK5 KD was lost in the presence of correctors. However, VX-445 had a deleterious effect on band C when knocking down GRK5, TPK1, DGKG on p.Phe508del-p.Gly550Glu-CFTR (**Fig.S6A**), suggesting a common, or a competing MoA at the NBD1:NBD2 pocket [14,41]. The p.Phe508del-4RK-CFTR revertant was additive to all kinase KDs, alone or in the

presence of correctors, except for TPK1 and GRK5, which produced unchanged (TPK1) or lower (GRK5) band C levels versus the drug alone. The DD/AA traffic variant was not affected.

Finally, we determined the specificity of hit kinases by assessing CFTR processing when performing kinase KDs in non-p.Phe508del-CFTR class II variants: p.Arg560Ser (legacy: R560S), p.Gly85Glu (legacy: G550E) and p.Asn1303Lys (legacy: N1303K) (**Fig.S7**). No rescue was observed, even in combination with CFTR folding correctors, indicating that the 5 kinases specifically regulate p.Phe508del-CFTR traffic.

GRK5 activity regulates p.Phe508del-CFTR PM localization and function

We considered the overall results obtained for the 5 hit kinases and selected GRK5 (G Protein-Coupled Receptor Kinase 5) for additional mechanistic studies, as KD of this kinase yielded the best p.Phe508del-CFTR rescue performance in most assays, including patch-clamp and WB. The likely overlap with the pathway targeted by VX-445 is potentially useful to describe its MoA regarding CFTR regulation. GRK5 has also been proposed as a therapeutic target for cardiovascular disorders [42], making it an attractive candidate for drug repurposing. Furthermore, GRK5 is a regulator of endogenous CFTR activation in the airway epithelium [43] through β_2 adrenergic receptor (β_2AR) signalling, acting at the level of receptor internalization, signal termination and cell desensitization [44]. Recently, the first GRK5-specific inhibitor was reported: 9g [45]. This 2-bromoacetylamido compound covalently binds GRK5 at low concentrations (IC_{50} = 8.6 nM) and with 1400-fold selectivity against the closely related paralog GRK2, thus being instrumental for complementing and validating the siRNA-based data.

To determine whether p.Phe508del-CFTR rescue could be obtained by inhibiting GRK5 with 9g, we started by performing a dose-response WB assay. CFBE cells expressing p.Phe508del-CFTR were incubated with 9g [0-1 µM] for 24h and band densitometry was compared with treatment with VX-661 (**Fig.7A**). Band C levels were the criterion used in the analysis of WB data because those are what really matters in terms of therapeutic benefit for people with CF, i.e., total amount of functional CFTR at the plasma membrane. We observed statistically significant band C rescue at 0.3 and 1.0 µM (50% of VX-661, **Fig.7B**), albeit without improved CFTR processing efficiency, due to a proportional increase in band B (**Fig.7C-D**). Higher 9g concentrations resulted in cellular toxicity and could not be used. Therefore, 1 µM was selected as the 9g concentration for further assays. To ascertain whether 9g is additive to CFTR correctors we incubated CFBE cells expressing p.Phe508del-CFTR with 1 µM 9g in the presence and absence of VX-661, VX-445 or VX-661 plus VX-445. WB analysis (**Fig.7E-H**) showed additivity of 9g to all corrector treatments, indicating a distinct MoA. Similarly, we performed HS-YFP quenching studies which also showed additivity in all conditions (**Fig.7I-J**).

To benchmark the effectiveness of p.Phe508del-CFTR rescue through GRK5 inhibition against the state of the art highly effective modulator combination (VX-445 plus VX-661 plus VX-770, or elexacaftor plus tezacaftor plus ivacaftor, ETI) we combined the modulator cocktail with either genetic or chemical GRK5 inhibition and investigated band C levels (**Fig. 7I-L**). Band C rescue is higher when using ETI (5.3-fold) than with either VX-809 (~2.8-fold over the control, **Fig. 5B**) or VX-661 (3.7-fold, **Fig. 5F**) in isolation. However, the combination VX-661 plus VX-445 – which omits VX-770 – yielded the highest extent of p.Phe508del-CFTR rescue: 7.0 (**Fig. 7F**).

Regardless, band C rescue by CFTR modulators is always further enhanced when applying genetic or chemical GRK5 inhibition (**Fig. 7**). This can be illustrated by a rescue extent of 7.8-fold under ETI (**Fig. 7J**) and 9.9-fold under VX-661 plus VX-445 (**Fig. 7F**), when 9g is used to inhibit GRK5. These results not only validated the p.Phe508del-CFTR rescue through GRK5 inhibition – since genetic and chemical inhibition with a drug-like molecule yield equivalent results – but also supported the hypothesis that GRK5 inhibition and current CFTR modulators rescue p.Phe508del-CFTR by distinct mechanisms.

GRK5 inhibition maximizes p.Phe508del-CFTR functional rescue in primary airway cells

To validate the biomedical relevance of pharmacological inhibition of GRK5 as a potential CFTR restoration strategy, we assessed its effects on primary Human bronchial epithelial (pHBE) cells from individuals with CF. We noticed that our batch of in-house synthesized 9g had limited long-term stability and did not meet chemical quality standards by the time we had established polarized pHBE cell cultures for Ussing chamber analyses. To overcome this limitation, we resorted to CCG-273441 (also known as 9j), an analogue of 9g, which inhibits GRK5 with equivalent performance ($IC_{50,\ 9g}$ = 8.6 nM, $IC_{50,\ 9j}$ = 3.8 nM; selectivity: $IC_{50,\ GRK2}/IC_{50,\ GRK5}$ = 1400 for 9g, $IC_{50,\ GRK2}/IC_{50,\ GRK5}$ = 1300 for 9j)[45] and can be obtained commercially (**Fig. S8A**). In CFBE cells expressing p.Phe508del-CFTR, 9j is trophic at low concentrations, boosting cellular metabolism and proliferation above the DMSO control (**Fig. S8B**). 9j rescued CFTR processing and ionic conductance in a manner additive to the VX-661 plus VX-445 combination (**Fig. S8C-H**), reaching significance after 48 h exposure to 300 nM 9j. At these conditions, cell viability was found to be 74%. No significant rescue was observed in the absence of modulators.

The functional effect of 9j was assessed by measuring CFTR-mediated chloride (Cl^-) transport in Ussing chamber using CF pHBE cells homozygous for p.Phe508del. This model was more tolerant to 9j and required slightly higher assay concentrations. Fully differentiated cells were pre-treated with VX-445/661 for 48 h, with 9j (500 nM) being added in the last 24h of the assay. Ussing chamber tracings (**Fig. 8A**) show a negative transepithelial voltage (V_{te}) deflection upon IBMX/Fsk and VX-770 stimulation in both VX-445/661 and VX-445/661/9j treated cells, indicating the activation of Cl^- secretion. The application of the specific CFTR inhibitor (CFTRinh-172), to confirm the induced ion transport is indeed CFTR-mediated, resulted in the reversal of the voltage direction in both conditions. When comparing the calculated equivalent short-circuit currents (Isc-eq) as presented in **Fig. 8B**, there is a trend toward an enhanced Cl^- Isc-eq when 9j is combined with VX-445/661 compared to the treatment with VX-445/661 alone. Focussing on CFTR-mediated current, i.e., the Isc-eq inhibited by CFTRinh-172[46-48], this was found to be significantly higher for VX-445/661/9j treated cells in comparison to cells treated with VX-445/661 alone, implying a higher CFTR-specific Cl^- transport in the presence of 9j. These results further confirm an additive effect of GRK5 inhibition to VX-445/661 by promoting CFTR rescue/trafficking to the cell surface and thus increasing CFTR function in primary CF airway epithelial cells.

Discussion

We describe here an siRNA-based HCS campaign aimed at identifying genes whose KD enhances p.Phe508del-CFTR PM levels. Given the residual amount of PM p.Phe508del-CFTR, a major challenge in this work was the establishment of imaging and image analysis protocols which could record such baseline levels (low intensity and, therefore, relatively noisy) and their modulation by siRNA or drugs. Validation of HCS results by orthogonal assays demonstrated the robustness of the screening method. After siRNA screening of nearly half of the human genome, selecting hit genes and re-screening them with different siRNAs we confirmed that 35 genes are key inhibitors of p.Phe508del-CFTR traffic as their KD enhances the PM localization of this CFTR variant. This stringent criterion equates to a 15% hit validation rate, somewhat lower than the 30% usually reported [33,34,49]. This can be explained by low siRNA efficiency or specificity and sub-optimal transfection efficiency (**Table S5**). As we demonstrate, this does not imply that hits identified in the primary screen which were not confirmed in the secondary screen should be excluded as playing a role in p.Phe508del-CFTR traffic, as demonstrated for GRK5, our top p.Phe508del-CFTR regulator which was a hit recovered from the primary screen, with sub-optimal scores in the secondary screen.

Through a combination of WB validation experiments, gene expression analysis and ERQC classification we identified 53 genes whose KD showed F508del-CFTR rescue in HCS or WB assays. The KD of the various hit genes had mixed effects on the sensitivity of CFTR to ERQC checkpoints, and it is therefore likely that they act by distinct MoAs. We noticed that besides affecting CFTR traffic and processing (*e.g.* WB band C), several hit siRNAs also affect the amount of immature p.Phe508del-CFTR (band B). In almost all cases we did not detect variations in CFTR mRNA expression (**Fig. S9A**) and thus attribute the regulation of band B amount to post-translational events. Among the hit genes that significantly increased levels of p.Phe508-CFTR at the PM (and band C) with the highest scores, were 5 kinases (TPK1, LRRK1, STYK1, GRK5, DGKG), which we selected for additional validation because of their potential druggability. The unique property of GRK5 of simultaneously being an ENaC inhibitor [33] is desirable for reversing CF symptoms in the clinic because the loss of Cl^- secretion via CFTR due to CF-causing variants is accompanied by Na^+ hyperabsorption via ENaC, which exacerbates airway dehydration [50,51].

To ascertain the biomedical relevance of inhibiting these kinases to achieve p.Phe508del-CFTR rescue we performed WB and patch-clamp assays in combination with treatment with clinical CFTR correctors VX-809 and VX-661. Data from WB show that p.Phe508del-CFTR rescue by GRK5 and LRRK1 KD was additive to that of corrector treatment, suggesting independent MoAs. The TPK1 KD may compete with corrector rescue mechanisms, as a decreased rescue was observed in the presence of corrector drugs. Rescue of p.Phe508del-CFTR by STYK1 and DGKG KD was not additive to corrector treatment, thus suggesting that they target the same mechanisms. In patch-clamp experiments the most significant rescue of p.Phe508del-CFTR function was achieved by GRK5 and LRRK1 KD, especially when combined with VX-809. We found that KD of the hit kinases was selective for p.Phe508del-CFTR versus other class II variants and that some of them could act through the first (Hsp70-mediated) ERQC checkpoint.

Altogether, we identified GRK5 as a new regulator of p.Phe508del-CFTR traffic and potentially relevant therapeutic target when inhibited, namely through pharmacological molecules 9g or 9j. This family of compounds is the first to selectively inhibit GRK5 vs e.g., GRK2. Initially, inhibition was thought to derive from irreversible covalent binding to the active site [45] but crystallographic data has since shown that binding is non covalent[52]. Low micromolar concentrations of 9g achieved significant rescue of p.Phe508del-CFTR traffic and function, which was additive to VX-809, VX-661, VX-661 plus VX-445 and the combination VX-770 plus VX-661 plus VX-445 (ETI), suggesting a potential added benefit. In this work, the highest extent of band C rescue occurred when combining 9g with VX-661 and VX-445 (9.9-fold over control). Rescue was lower under ETI (7.8-fold), which we attribute to the well documented inhibitory effect of VX-770 on p.Phe508del-CFTR rescue when used in a chronic setting together with either VX-809[53,54], VX-661[54] or VX-664 plus VX-445[55].

Despite being able to rescue band C, and additive with folding correctors towards processing (WB) and functional (HS-YFP) rescue, 9g or 9j alone were ineffective in rescuing p.Phe580del-CFTR function (**Fig. 7 M-N**). We interpret this observation as these inhibitors acting as correctors of p.Phe508del-CFTR trafficking but not of its gating defect. Based on WB data, 9j may effectively work as a "CFTR amplifier", i.e., by exposing more CFTR molecules to modulator correction. We believe the additivity (*i.e.* distinct MoA) with CFTR correctors derives from the fact that the latter modulators bind specific pockets in the CFTR polypeptide[13] whereas GRK5 inhibitors are expected to act in an indirect manner, likely through modulation of CFTR molecular interactions. Regardless, the GRK5 inhibitor phenotype is always statistically significant when used in combination with p.Phe508del-CFTR folding correctors. Primary cell studies required 9j, a more potent – and perhaps more stable – GRK5 inhibitor than 9g. Again, we found that the inhibition of GRK5 in pHBE cells was fully additive to folding correctors in the restoration of p.Phe508del-CFTR PM levels and its chloride conductance.

The most likely MoA by which GRK5 inhibition rescues p.Phe508del-CFTR is through the well-established pathway of endogenous activation through β_2AR [56,57] (**Fig. 9**). β_2AR is a G-protein coupled receptor (GPCR) and binding of extracellular β_2AR agonists (*e.g.* epinephrine) is transduced intracellularly through trimeric G proteins, which activate adenylyl cyclase, the enzyme which converts ATP into cyclic AMP (cAMP) [58]. Indeed, cAMP contributes to functionally activate CFTR through two independent pathways: activation of protein kinase A (PKA) which phosphorylates CFTR R domain (RD) as the first step in channel gating [59]; and EPAC1-dependent stabilization at the PM through tethering to NHERF1 [60]. Termination of the adrenergic signal is dependent on GPCR kinases (GRK). Humans express 7 GRK isoforms (GRK1-7) [61] which selectively bind the cytoplasmic face of ligand-bound – *i.e.* activated – GPCRs to phosphorylate Ser/Thr residues [62,63]. Phosphorylated GPCRs become high-affinity targets for arrestins, which shield the cytoplasmic face of the receptor, preclude further G-protein binding and activation and induce receptor endocytosis. Eventually, receptors are recycled to the PM to restore cell sensitization. The most well-studied GRKs are GRK2 and GRK5, two important therapeutic targets, as their inhibition can prevent heart failure and hypertrophic cardiomyopathy [64].

Although it is still unclear how GRK5 inhibition releases p.Phe508del-CFTR from the ER, available CFTR interactomes seem to rule out a direct GRK5-CFTR interaction. Thus, the existence of additional mediators is most likely since no ER functions have yet been ascribed to GRK5. Interestingly, β_2AR has been identified in a

macromolecular complex tethering CFTR to the PM via NHERF1 through PDZ-based interactions [43], even though GRK5 involvement was not probed. Additionally, β_2AR stimulation in airway epithelial cells enhances CFTR activity [43]. Despite several reports relating GRK5 expression levels with neurodegenerative, cardiovascular and metabolic diseases[65] we have not found significant alterations in GRK5 mRNA when comparing cells expressing wt- or p.Phe508del-CFTR (**Fig. S8B**) or across DMSO versus 9g or ETI. We interpret this observation as the regulation of CFTR traffic and intracellular localization through GRK5 being due to dysregulated signalling events and not altered GRK5 expression. It is also unclear whether the possible impact on the cellular cAMP pool may be part of the GRK5 MoA. Endogenously, GRK5 is activated by interaction with Ca^{2+}-calmodulin, a process which can be inhibited with malbrancheamide [66]. This contribution was not assessed in this work because that would be a target upstream GRK5.

Our results identify GRK5 as a putative novel therapeutic target for Cystic Fibrosis, which can be inhibited with the selective inhibitors 9g or 9j to maximize p.Phe508del-CFTR rescue by current approved corrector drugs, including the highly effective modulator therapy combining ETI. The additivity of 9g/9j with CFTR modulators points to an independent MoA and a potential new pharmacological manoeuvre to augment CFTR function in the majority of individuals with CF. The low or sub-micromolar range where we observed rescue is at the same range as CFTR clinical correctors, indicating good potency. Available data on GRK5 and β_2AR may provide a useful framework to further examine additional potential non-PM functions of GRK5 and the mechanistic connection between GRK5 inhibition and CFTR traffic regulation through this new druggable target.

Resource Availability

Lead contact

Further information and requests for resources and reagents should be directed to and will be fulfilled by the lead contact, Margarida D. Amaral (mdamaral@ciencias.ulisboa.pt).

Materials availability

This study did not generate new unique reagents.

Data and code availability

- Primary and secondary high content screening data have been deposited at Zenodo and are publicly available as of the date of publication. DOIs are listed in the key resources table.
- All original code has been deposited at Zenodo and is publicly available as of the date of publication. DOIs are listed in the key resources table.
- Any additional information required to reanalyze the data reported in this paper is available from the lead contact upon request.

Limitations of the study

Some of the limitations of our study stem from the RNAi HCS methodology. Our screening library only covered about half of the human genome. This not only limits the overlap (and the ability to compare our results) with previous works but also raises the possibility that we may have missed to detect relevant CFTR regulator genes. Despite being a highly relevant CF model system, the cellular assay we used for the HCS assay might not feature all *in vivo* CFTR regulatory mechanisms and, therefore, not enable discovering all CFTR traffic regulator genes. siRNA-based assays – especially high-throughput assays, where transfection conditions cannot be optimized for all targets – commonly feature an inherently incomplete gene silencing, which is also the case for our study. This effect is likely to reduce the sensitivity to detect weaker or redundant CFTR regulators and can be overcome by shRNA nor CRISPR/Cas9-based assays. It is possible that 9g can also be used effectively in the laboratory at incubation times other than the one we used (24 h). Finally, 9j dose-response was not exhaustively probed in pHBE epithelial cells, and there might exist experimental conditions which enhance CFTR rescue further than herein reported.

Acknowledgements

Work supported by UIDB/04046/2020 (DOI: 10.54499/UIDB/04046/2020) and UIDP/04046/2020 (DOI: 10.54499/UIDP/04046/2020) Centre grants from FCT, Portugal (to BioISI)., UIDB/00100/2020 and UIDP/00100/2020 (to CQE) from FCT—Fundação para a Ciência e a Tecnologia, Portugal and research grants (to MDA): TargetScreen2-FP6-2005-LH-7-037365 (European Union); PTDC/SAU-GMG/122299/2010 (FCT, Portugal); Ref. 7207534 (CFF, USA) and (to HMB) NewKinCF 2022.03453.PTDC (DOI: 10.54499/2022.03453.PTDC, FCT, Portugal). MCP was recipient of a fellowship (SFRH/PD/BD/114393/2016) from BioSys PhD programme PD/00065/2012, from FCT, Portugal. HMB held a Junior Researcher Contract from FCT (DOI: 10.54499/DL57/2016/CP1479/CT0012). MLP is a recipient of the 2018 Gilead Sciences Research Scholars for Cystic Fibrosis. VC was recipient of a research contract funded by the PTSense research grant (AMARAL19G0) from CFF, USA (to MDA). HCS was performed at the EMBL Advanced Light Microscopy Facility and Faculty of Sciences of the University of Lisboa Microscopy Facility, a node of the Portuguese Platform of BioImaging (PPBI), PPBI-POCI-01-0145-FEDER-022122 from FCT.

The authors are grateful to Dr. Nicoletta Pedemonte for providing the primary bronchial epithelial cells for this study.

Author Contributions

Conceptualization: HMB, MLP, MCP, BN, CM, KK, RP, MDA.

Methodology: HMB, MLP, MCP, VC, CT, MDA.

Software: HMB, CT.

Validation: HMB, MLP, MCP, VR, MFC, MDA.

Formal analysis: HMB, MLP, MCP, VR, MFC, JO, LAC.

Investigation: HMB, MLP, MCP, VR, IP, MFC, LAC, VC, JO.

Resources: HMB, VC, KK, RP, MDA.

Data curation: HMB.

Writing – original draft: HMB, MDA.

Writing – review and editing: All authors.

Visualization: HMB, MLP, MCP, VR, MFC.

Supervision: HMB, IP, BN, CT, CM, KK, RP, MDA.

Funding acquisition: MDA, HMB.

Declaration of Interests

HMB, MLP and MDA are inventors in the international patent PCT/IB2023/051813 filed by the Faculty of Sciences of the University of Lisboa at the World Intellectual Property Organization which protects targeting the GRK5 or LRRK1 genes or proteins to rescue p.Phe508del-CFTR.

Main Figure Titles and Legends

Figure 1. Workflow of siRNA-based p.Phe508del-CFTR traffic screens. (A) The primary HCS was based on screening the Ambion extended druggable genome siRNA library (9126 genes, each targeted by 3 individual siRNAs) with a CFBE cell line expressing the mCherry-Flag-p.Phe508del-CFTR traffic reporter. An siRNA subset was discarded due to off-target effects or failed assay plate preparation. The primary screen highlighted 228 hit siRNAs – targeting 227 genes – which produced significant increases in p.Phe508del-CFTR PM delivery. Most primary hits (225 genes) were re-screened with additional siRNAs (2 siRNAs/gene). A total of 35 gene hits, targeted by 70 siRNAs, were confirmed. For validation, an siRNA library targeting the 35 confirmed hit genes as well two additional kinases (DGKG, GRK5) which were among the primary hits was assembled. Significant increases in p.Phe508del-CFTR glycosylation (Western blot) or function (HS-YFP) were achieved by knocking down, respectively, 34 or 21 of the 37 genes. The overlap between YFP and WB is 20 genes and 25 siRNAs. Downstream studies focused on 5 kinases, selected for their druggability. GRK5 was selected as the best hit and additional studies with a specific small molecule inhibitor were performed. In parallel, reporter cell lines expressing wt-CFTR, the DD/AA-CFTR variant or genetic p.Phe508del-CFTR revertants affecting ERQC checkpoints were used to screen the confirmation siRNA library, thereby classifying hit genes according to their dependence on different ERQC mechanisms. For simplicity, the summary matrix uses single letter amino acid codes. (B) Waterfall plot with Z-score$_{5\times5}$ for PM p.Phe508del-CFTR (median ± SEM) obtained with all siRNAs analyzed in the primary screen and (C) inset showing the subset of 228 primary siRNAs which significantly increase PM p.Phe508del-CFTR. Dotted lines show the positive (Z-score$_{5\times5}$ > +1), negative hit threshold (Z-score$_{5\times5}$ < -1), or the readout for cells treated with 3 µM VX-809. For most siRNAs n=3 biological replicates (see **Dataset S1**).

Figure 2. Overview of the confirmation siRNA screen. (A) Waterfall plot of p.Phe508del-CFTR PM localization Z-scores. Values are median ± SEM. Negative (Z-score < 1). Negative and positive hits are shown in red or green, respectively. Selected positive hits from panel B are shown. (B) Representative microscopy images of controls and selected hit genes. Neg1 is the non-targeting siRNA used as negative control for Z-score calculation. Neg2 is another non-targeting siRNA which yields CFTR PM Z-score close to the baseline. VX-809 (3 µM) was added to selected wells containing Neg1 as a positive control. The loss of CFTR expression (mCherry) in CFTR siRNA-treated cells reports on a high transfection efficiency. Gene symbols, the respective siRNAs catalogue numbers and median Z-scores are shown. Scale bar: 50 µm. (C) Z-score for the PM and traffic efficiency quantification, shown as median ± SEM. For most siRNAs n=3 biological replicates (see **Dataset S3**).

Figure 3. Effect of hit siRNAs on p.Phe508del-CFTR processing assessed by WB. (A) CFBE cells overexpressing p.Phe508del-CFTR were transfected with siRNAs targeting 34 of the 35 confirmed hit genes (LDLRAD could not be included) and analyzed by WB for processing to confirm effects on CFTR traffic rescue. Wt-CFTR was included for reference. Densitometric quantification of the fully glycosylated band C (B), immature, core glycosylated band B (C) and CFTR processing [C/(B+C)] (D), normalized to the corresponding loading controls (mean ± SD). ´*´ indicates statistical significance from Neg1-treated cells ($p<0.05$, one-way ANOVA followed by Dunnett's post-hoc test, n=3 biological replicates). Of the 68 tested siRNAs, 58 showed significant band C rescue and 27 showed significantly increased processing. For 26 siRNAs simultaneous increases in band C and processing were observed. Gel lanes were reordered and juxtaposed for presentation consistency and clarity.

Figure 4. Quantification of CFTR function through the HS-YFP quenching assay. CFBE cells expressing p.Phe508del- or wt-CFTR were transfected with siRNAs targeting the 53 confirmed hit genes and ionic transport was measured via the HS-YFP quenching assay. Gene targets and siRNA IDs are shown. Plot values are quenching rate Z-score versus the negative control (mean ± SD, n = 2-8 biological replicates). Vertical gray lines mark the Z=1 threshold applied for hit identification. Hit siRNAs for p.Phe508del-CFTR function rescue are shown with arrows. Numerical data available in Dataset S5.

Figure 5. Additivity of hit kinase KD with CFTR correctors on p.Phe508del-CFTR processing rescue. CFBE cells expressing p.Phe508del-CFTR were transfected with Neg1 or siRNAs targeting STYK1, TPK1, DGKG, GRK5 or LRRK1 and incubated for 24h with DMSO (vehicle), 3 µM VX-809 (A-D) or 5 µM VX-661 (E-H). Representative WB membranes (A, E) and densitometric quantification of CFTR and C normalized to the calnexin loading control (B-D and F-H). ´#´ indicates statistical significance from the corresponding DMSO control ($p < 0.05$ in double-tailed unpaired t-test, n=3 biological replicates). Plot values are mean ± SD. Gel lanes were reordered and juxtaposed for presentation consistency and clarity.

Figure 6. Whole cell currents of CFBE cells overexpressing p.Phe508del-CFTR and treated with siRNAs targeting hit kinases. (A) Whole cell overlay currents (Vc = ± 100 mV, steps 20 mV) activated by 25 µM Genistein + 2µM Fsk (Gen/Fsk) in CFBE wt-CFTR cells (non-treated) or CFBE p.Phe508del-CFTR cells transfected with Neg1 or siRNAs targeting STYK1, DGKG, TPK1, GRK5 or LRRK1 with and without incubation for 24h with 3 µM VX-809. (B) Current/voltage (I/V) curves -100 mV to +100 mV for each siRNA in Ringer (white) or after stimulation with 25 µM Genistein + 2µM Fsk (Gen/Fsk) (black). All solutions contained 50 nM TRAM 34, a potassium (K^+) channel inhibitor to discard K^+ currents and the number (n) of experiments is indicated in each graph. (C) Current densities obtained at Vc = +100 mV. Delta of the average of Gen/Fsk-induced current densities. '$' indicates statistical significance of Gen/Fsk-stimulated currents of the respective siRNA vs Neg1 ($p<0.05$ in unpaired t-test), '#' siRNA+VX-809 vs Neg1+VX-809 ($p<0.05$ in unpaired t-test), '*' siRNA control vs

siRNA + VX-809 ($p<0.05$ in unpaired t-test). Values are mean ± SD. Numbers within parenthesis are the replicate count. ND: Not detected.

Figure 7. GRK5 inhibition with 9g rescues p.Phe508del-CFTR traffic and function. (A) CFBE cells stably expressing p.Phe508del-CFTR were incubated with increasing doses of 9g or VX-661 3 μM and analyzed with WB. Densitometric quantification of band C (B), band B (C) and CFTR processing [C/(B+C)] (D). Significant band C rescue is observed at 0.3 and 1.0 μM of 9g. Processing is not affected due to proportional band B increases. Symbols indicate statistical significance from DMSO ("#") or VX-661 ("*") lanes ($p<0.05$, one-way ANOVA followed by Dunnett's post-hoc test, n=3 biological replicates). (E) Additivity of 9g (1 μM) to CFTR correctors VX-661 (5 μM), VX-445 (3 μM) and VX-661 + VX-445 and densitometric quantification of band C (F), band B (G) and processing (H). 9g is additive to all corrector treatments regarding bands C and B (# $p<0.05$ double-tailed unpaired *t*-test, n=4 biological replicates). (I) Additivity of 9g (1 μM) to the triple combination of compounds which comprise the highly effective CFTR modulator therapy: VX-661 (5 μM), VX-445 (3 μM) and VX-770 (3 μM) and densitometric quantification of band C (J), band B (K) and processing (L). The modulator cocktail significantly rescues p.Phe508del-CFTR on all WB measurements. Furthermore, GRK5 inhibition with siRNA (GRK5) or 9g is additive to ETI treatment regarding band C and CFTR processing. Symbols indicate statistical significance from matching DMSO ("#", $p<0.05$, double-tailed unpaired *t*-test, n=4 biological replicates) or ETI alone experiments ("*", $p<0.05$, one-way ANOVA followed by Dunnett's post-hoc test, n=4 biological replicates). (M) HS-YFP quenching of CFBE cells expressing p.Phe508del-CFTR and incubated with 9g (1 μM) and/or VX-661 (5 μM), VX-445 (3 μM) and VX-661 + VX-445. (N) Quenching rate at the moment of iodide addition. 9g is additive to all corrector treatments regarding p.Phe508del-CFTR functional rescue (# $p<0.05$ double-tailed unpaired t-test, n=4 biological replicates). All plot values are mean ± SD. Gel lanes were reordered and juxtaposed for presentation consistency and clarity.

Figure 8. Effect of 9j on CFTR function in primary CF human bronchial epithelial (pHBE) cells. (A) Representative Ussing Chamber recordings of chloride transport measured as transepithelial voltage (Vte). Vte and transepithelial resistance (Rte) were recorded and used to calculate the equivalent short-circuit current (Isc-eq) using Ohm's law: Isc-eq = Vte/Rte, as previously reported [67]. Fully differentiated pHBE cells homozygous for p.Phe508del were pre-treated with a combination of 3 μM VX445 and 5 μM 661 for 48h and additionally with DMSO (vehicle) or 500 nM 9j in the last 24h of assay. Amiloride (ENaC channel inhibitor) was added apically, followed by a combination of IBMX and Fsk (cAMP-elevating agents), VX-770 (CFTR potentiator), and Inh172 (CFTRinh-172, CFTR specific inhibitor). (B) Summary of calculated equivalent short-circuit currents (Isc-eq) induced by IBMX/Fsk + VX-770 and inhibited by Inh172. Values are represented as mean ± SD (n = 7 biological replicates). * represents significance (p-value <0.05, unpaired *t*-test).

Figure 9. Model for p.Phe508del-CFTR rescue via GRK5 inhibition. GRK5 is part of the machinery which activates CFTR endogenously, in response to β_2-adrenergic receptor (β_2AR) ligands such as epinephrine,

isoprenaline or albuterol. Ligand binding is transduced intracellularly by the hetero-trimeric G proteins associated with β_2AR, which activate adenylyl cyclase. The resulting cAMP pool increase activates CFTR by: (i) PKA activation, which phosphorylates CFTR's R and initiates the gating cycle which opens the channel, and (ii) EPAC1-dependent stabilization of CFTR at the PM. Adenylyl cyclase can be artificially activated with forskolin (Fsk). The cAMP pool is depleted by phosphodiesterases (PDE), which can be inhibited with 3-Isobutyl-1-methylxanthine (IBMX). GRK5 phosphorylates activated β_2AR, which then becomes substrate for β-arrestin and is endocytosed to interrupt receptor signaling. Endocytic vesicles are recycled to the PM to restore cell sensitization. GRK5 kinase activity is promoted by Ca^{2+}-calmodulin (CaM). GRK5 inhibition with siRNAs, 9g or 9j releases p.Phe508del-CFTR from the ER, increases the steady state at the PM and yields higher CFTR-dependent Cl^- conductance, both in airway cell lines and primary cells. The link between GRK5 and p.Phe508del-CFTR ER release is not completely clear but given that GRK5 is not a CFTR interactor and its inhibition is additive to VX-661 a direct GRK5-CFTR mechanism is unlikely. Adapted from [56,57].

STAR★Methods

EXPERIMENTAL MODEL AND STUDY PARTICIPANT DETAILS

Bronchial epithelial cell lines

mCherry-Flag-CFTR with Tet-ON expression in CFBE41o$^-$ cells were described elsewhere [26,68], representing wt- and p.Phe508del-CFTR[26], p.Phe508del revertant variants p.Phe508del-4RK (p.Arg29Lys, p.Arg516Lys, p.Arg555Lys, p.Arg766Lys), p.Phe508del-p.Arg1070Trp-CFTR, p.Phe508del-p.Gly550Glu-CFTR, and DD/AA-CFTR[29]. Cells were grown in DMEM containing 4.5 g/L Glucose and L-Glutamine (Lonza, #12-604F) supplemented with 10% FBS (Gibco #10106), 2 µg/ml puromycin (Sigma-Aldrich, # P8833) and 10 µg/ml Blasticidin (InvivoGen, #ant-bl) at 37°C in 5% CO_2. CFBE41o$^-$ cells constitutively co-expressing HS-YFP (YFP-H148Q/I152L) and wt- or p.Phe508del-CFTR[69] were a kind gift from Dr Nicoletta Pedemonte (IRCCS Istituto G. Gaslini, Genoa, Italy). Cells were cultured in MEM supplemented with 10% FBS, 2 mM L-glutamine, 2 µg/ml puromycin and 200 µM G418 (Sigma-Aldrich, # A1720) at 37°C in 5% CO_2. CFBE41o$^-$ cells constitutively expressing wt- or p.Phe508del-CFTR [70] were grown in DMEM, 10% FBS and 2 µg/ml puromycin at 37°C in 5% CO_2.

Primary human bronchial epithelial cells

Primary human bronchial epithelial cells (pHBE), obtained from one p.Phe508del/p.Phe508del CF individual, were kindly provided by Dr. Nicoletta Pedemonte, IRCCS Istituto Giannina Gaslini, Genova, Italy. pHBE cells were cultured and expanded in Pneumacult ExPlus media according to the manufacturer's protocol (StemCell Technologies) and seeded on collagen-type I-coated (30 µg/mL, Advanced Biomatrix, 5005) porous inserts (Transwell®, Corning, USA). After reaching confluency, cells were differentiated in Pneumacult-ALI media (StemCell Technologies) for 28 to 42 days in air-liquid interface (ALI) conditions. Then, CFTR-mediated Cl^- transport was assessed in cells exposed to CFTR modulators (VX-445 plus VX-661), with and without GRK5 inhibitor 9j (see "Ussing Chamber recordings" below). A total of 7 inserts were assayed for each condition.

Ethics Statement

The collection of bronchial epithelial cells (supported by Fondazione per la Ricerca sulla Fibrosi Cistica through the "Servizio Colture Primarie") and their study to investigate the mechanisms of transepithelial ion transport were specifically approved (on 8 July 2018) by the Ethics Committee of the IRCCS Istituto Giannina Gaslini following the guidelines of the Italian Ministry of Health (registration number: ANTECER, 042-09/07/2018). Each patient provided informed consent to the study using a form that was also approved by the Ethics Committee.

METHOD DETAILS

Chemicals

VX-445 (#S8851), VX-661 (#S7059), VX-770 (#S1144) and VX-809 (#S1565) were purchased from Selleckchem, USA. Amiloride, 3-isobutyl-1-methylxanthine (IBMX, #I5879), Forskolin (#F6886) were purchased from Sigma-Aldrich, USA. CFTRinh-172 (#HY-16671) and CCG-273441 (9j, #HY-47573) were purchased from MedChemExpress, USA. 9g (CCG-273463) was synthesized in-house, as described below.

siRNA libraries

The primary screen used the Ambion Silencer Human Extended Druggable Silencer siRNA library laid out in 384 well plates [27]. Only siRNAs targeting a single protein-coding gene (as of Ensembl78) were considered. Plate coating with siRNAs (described in [26]) failed in 8 plate layouts, which were discarded. Primary screen hits were re-screened with a cherry-picked Ambion Silencer Select siRNA library (2 siRNAs per gene target) using the same coating protocol. Validation assays (WB and HS-YFP quenching) used siRNAs from the secondary screening library and the same coating protocol.

CFTR traffic assay: primary screen

To establish an assay compatible with siRNA-based gene KD and small molecule treatments, a total experiment time of 72 h was selected, a consensus time in other studies [6,71]. In the primary screen CFTR intracellular localization was assessed in CFBE cells expressing the inducible mCherry-Flag-p.Phe508del-CFTR traffic reporter and subjected to siRNA KDs. Cells were split 24h before the start of the experiment to synchronize them in exponential growing phase and maximize transfection efficiency. The experiment was initiated by seeding cells in transfection-ready microscopy-grade multi-well plates [72]. At the moment of CFTR induction the siRNA target gene is – at least partially – absent. Each well was seeded with 2,500 cells using a peristaltic pump (ThermoFisher Multidrop™ Combi) in the absence of antibiotics. Expression of mCherry-Flag-p.Phe508del-CFTR was induced with 1 µg/ml doxycycline (Dox, Sigma-Aldrich, #9891) starting at 24 h after seeding and continuing for 48 h, to allow for sufficient construct expression (mCherry fluorescence). The positive controls were wells containing a non-targeting siRNA (Scrambled), induced with 3 µM VX-809 and 0.1% FBS.
After the 72h assay time, immunofluorescence was performed to detect extracellular Flag tags in non-permeabilized cells [26,27]. Briefly, cells were washed once in ice cold PBS supplemented with 0.7 mM $CaCl_2$ and 1.1 mM $MgCl_2$ (PBS^{++}), incubated 1 h with an anti-Flag antibody (1:500, Sigma-Aldrich #F1804), washed three times with ice cold PBS^{++}, incubated 20 min with 3% paraformaldehyde (PFA), washed three times with room temperature PBS^{++}, incubated 1 h with an anti-mouse Alexa Fluor 647 conjugated secondary antibody (1:500, Invitrogen #A31571), washed three times with PBS^{++}, incubated with Hoechst 33342 (200 ng/ml, Sigma #B2261) for 1 to 6 hours, washed with PBS^{++} and stored at 4°C until imaging. Antibodies were solubilized in PBS^{++} containing 1% BSA (Aldrich #A9647). PFA and Hoechst were solubilized in PBS^{++}.

CFTR traffic assay: secondary screen

The 227 primary screen hit genes were re-screened with 2 additional siRNAs using the traffic assay described for the primary screen and CFBE cells expressing the mCherry-Flag-p.Phe508del-CFTR reporter. siRNAs with

improved stability and specificity (Ambion Silencer Select) and different sequences than the ones in the primary screen were used (see siRNA libraries).

CFTR traffic assay: ERQC checkpoints classification screen

Classification of the primary screen hits in terms of their effect on the ERQC checkpoints which retain p.Phe508del-CFTR was pursued by re-screening the primary screen hits using the reporter cell lines expressing wt-CFTR, p.Phe508del-CFTR genetic revertants (4RK, p.Gly550Glu or p.Arg1070Trp) as well as the DD/AA variant.

Image acquisition

The imaging workflow was based on preliminary experiments performed on an Olympus ScanR widefield system [26]. Imaging was performed at room temperature with a Leica DMI6000 B inverted epifluorescence microscope equipped with a metal halide light source (EL6000), a 10x NA 0.40 HC PL APO objective, a Hamamatsu Orca-Flash4.0 CMOS camera and Leica Microsystems filter cubes suitable for imaging the fluorophores used in the traffic assay: Hoechst 33342 (model A: excitation: BP 340-380; dichroic mirror 400; emission filter LP 425;), mCherry (model N2.1: excitation BP 515-560; dichroic mirror 580; emission LP 590) and Alexa Fluor 647 (custom: excitation: BP 630-660; emission LP 670). The microscope was controlled by the Leica MatrixScreener software, using software autofocus and 4 image fields per well. Images were metadata annotated and organized with the R package htmrenamer[73] and stored as 16 bit OME-TIFF.

Image analysis

Image quantification was performed with CellProfiler (http://cellprofiler.org/)[74], including dark field / flat frame background correction, cell segmentation, fluorescence integration and basic quality control (exclusion of cells undergoing mitosis, apoptosis or containing a significant amount of saturated pixels). Three cell-based features were extracted: integrated mCherry fluorescence signal (total CFTR expression), integrated Alexa Fluor 647 fluorescence (amount of CFTR molecules inserted into the PM) and the ratio of the integrated fluorescence signals from Alexa Fluor 647 and mCherry (A647/mCherry, CFTR traffic efficiency). Hit thresholding was based on the PM signal. The secondary and classification library plates contained 5-8 wells with siRNA targeting CFTR, as transfection control. Only plates where mCherry fluorescence was lost (*i.e.* abrogation of CFTR expression) in the majority of cells were scored.

Data analysis – primary screen

The PM CFTR phenotype generated by each siRNA was scored through R scripts. The algorithm takes as input image-based features (*e.g.* metadata, focus score, background fluorescence) and cell-based features (*e.g.* the image they belong to, metadata, fluorescence intensities, traffic efficiency ratio) generated by image analysis with CellProfiler and computes a modified Z-score for the PM fluorescence intensity and traffic efficiency ratio produced by each siRNA. The algorithm has been implemented in the R programming language and has the following steps: *i)* Import image and cell features; *ii)* Quality Control: exclude data from unapproved plates (bad sample preparation), wells (wells with less than 100 cells), images (out-of-focus or high background

images) and cells (aberrant morphology, fluorescence saturation or low CFTR expression); *iii)* Well Summary: take the PM fluorescence intensity and traffic efficiency values for all cells in a well and compute their respective medians; *iv)* Normalization: convert each well summary value into a score. Due to the lack of reliable non-targeting siRNAs in the primary screen library, the negative control measurements for each well were provided by neighbouring ones, as defined by a 5×5 matrix centred at the target well. For external wells, which do not have 24 neighbours, missing values were dropped. Data was normalized with a modified Z-score defined by:

$$\text{Modified Z-score} = \frac{x - Median\left(Neighbors_{5\times5,plate_i}\right)}{sd\left(Neighbors_{5\times5,plate_i}\right)}$$

where *x* is the well summary value, *sd* is the standard deviation and $Neighbors_{5\times5,plate_i}$ is the ensemble of negative control values; *v)* Plate summary: compute the median of the normalized PM staining and traffic efficiency values for all wells which have the same siRNA treatment in the same plate; *vi)* Treatment summary: take the plate summary values and compute their median across replicate plates. The median-summarized values are the ones we report in this publication.

Data analysis – secondary and classification screens

In the secondary and classification libraries 10 to 18 wells in each 384 well plate contained a non-targeting siRNA (Neg1) as negative control. Data was analyzed as in the primary screen, with two differences: (i) also discarding plates with low transfection efficiency in wells containing CFTR siRNA; and (ii) using a standard Z-score at the normalization step, using the average and standard deviation of wells containing the non-targeting Neg1 siRNA.

Halide-sensitive YFP fluorescence quenching

The assay followed an established protocol[69]. For siRNA-based assays, CFBE cells co-expressing HS-YFP and wt- or p.Phe508del-CFTR were grown to confluency and split to 50%. On the following day, the experiment was initiated by seeding cells onto siRNA-coated 96 well plates using a peristaltic pump (10,000 cells/well, in antibiotic-free medium). 48 h later, VX-809 (3 µM) or VX-661 (5 µM) were added to selected wells containing Neg1 siRNA in reduced FBS (0.1%). 72 h after seeding (as in microscopy-based screens), cells were washed two times with PBS (containing 137 mM NaCl, 2.7 mM KCl, 8.1 mM Na_2HPO_4, 1.5 mM KH_2PO_4, 1 mM $CaCl_2$, and 0.5 mM $MgCl_2$) and stimulated for 30 min with PBS containing Forskolin (20 µM) and VX-770 (3 µM) at 37°C under atmospheric CO_2. Each well was added 60 µl of the stimulation solution. After stimulation, each plate was transferred to a fluorescence plate reader equipped with fast injectors (Tecan Infinite F200 Pro) and YFP excitation (BP 475-495 nm) and emission (BP 523-458 nm) filters. Each assay consisted of a continuous 16 s fluorescence reading with 2 s before and 14 s after injection of 160 µl of a PBS where Cl^- had been replaced by I^- (final I^- concentration in the well: 100 mM). The pH of all PBS-containing solutions was rigorously set at pH 7.4 immediately before use to avoid artifacts in the fluorescence reading. Kinetic data was background subtracted and normalized to the pre-injection value. The final 14 s of the kinetics in each well were fitted with a single decay exponential curve and the derivative at the injection time (*i.e.* the quenching rate) was extracted from the curve parameters. The negative of the quenching rate was converted to Z-score or fold

change versus the negative control. For 9j assays, p.Phe508del-CFTR expressing cells were grown in MEM with 10% FBS and seeded at 18,500 cells/well. 9j and modulators were added 24 h later, in reduced FBS medium (1%) and were incubated for 48 h (replacing with fresh identical medium midway).

Western Blotting (WB)

Assays used CFBE cells constitutively expressing wt-, p.Phe508del-, p.Phe508del-p.Gly550Glu-, p.Phe508del-p.Arg1070Trp-, p.Phe508del-4RK-, DD/AA-, p.Gly85Glu- or p.Asn1303Lys-CFTR. Confluent cell cultures were split to 50% confluency, to stimulate cell proliferation and enhance transfection efficiency. 24 h later, cells were seeded into 12-well plates which had been coated with siRNAs for reverse transfection (87,500 cells/well). The plate coating protocol was the same as for the microscopy screening assay. Each plate included a non-targeting Neg1 siRNA as negative control and a CFTR targeting siRNA as transfection control. Cells were grown for 48 h in the presence of siRNAs. When required, VX-809 (3 µM), VX-661 (5 µM), VX-445 (3 µM) or VX-770 (3 µM) were added in the last 24 h of siRNA contact – alone or in combination, as required – along with matching DMSO controls. 9j response assays used CFBE cells expressing p.Phe508del-CFTR seeded at a density of 110,000 cells/well in 24 well plates and grown in MEM media. 24h after seeding, cells were exposed to DMSO or VX-661 plus VX-445 in combination with 9j at several concentrations for 24 or 48 h. In 48 h incubation studies, the culture medium was replaced with fresh and identical medium at the incubation midpoint.

WB samples were prepared by lysing transfected cells with Laemmli sample buffer. The buffer contained no bromophenol and was supplemented with a protease inhibitor cocktail (Roche, Complete: one tablet per ml), benzonase and magnesium chloride. Cells were scrapped manually at 4°C and lysates were stored at -20 °C until analysis. Following quantification, the same protein amount of each lysate was loaded on SDS-PAGE gels (7.5% or 10%), electrophoresed, blotted and probed with anti-CFTR (CFFT 596, 1:1000-1:3000) or anti-Calnexin (BD Transduction Laboratories #610523, 1:3000) antibodies. Membranes were developed with a luminescent enzymatic reaction. wt-CFTR samples had lower concentration to allow proper visualization of the much more abundant CFTR bands.

Images were quantified with Bio-Rad's Image Lab software, with local background subtraction. Band densitometry was initially transformed into fold change versus the loading control. To compare across bands, results were reported as fold change versus p.Phe508del-CFTR-expressing cells transfected with the Neg1 siRNA without correctors.

Cell viability assay

To assess cell viability using a metabolic reporter, we used the resazurin reduction assay. CFBE cells expressing p.Phe508del-CFTR were cultured on MEM supplemented with 10% FBS and seeded on 96 well clear bottom plates (Greiner #655090), at a density of 18,500 cells/well. 24 hours later, culture media was replaced MEM supplemented with 1% FBS and either DMSO or VX-661 (5 µM) plus VX-445 (3 µM) plus 9j (0 to 30 µM). Cells incubated for a total of 48 h, with compounds being refreshed at the incubation midpoint. After the incubation, 5 wells on each plate were exposed to 30% ethanol for 20 s, to provide a 0% viability control. Then, cells were incubated with 10 µg/ml resazurin (Sigma-Aldrich # R7017) on DMEM supplemented with 1% FBS

for 1 h at 37°C. Fluorescence (excitation 531/40 nm; emission 595 nm) was measured on a Victor 3V plate reader (PerkinElmer). Viability was computed using the 0% (ethanol) and 100% (DMSO vehicle) controls. The 9j EC50 was determined through a logistic fit to the concentration-dependent data.Patch-clamp.

The p.Phe508del-CFTR chloride conductance was investigated in CFBE cells overexpressing p.Phe508del-CFTR and transfected with the following Ambion Silencer Select siRNAs against selected hit genes: siDGKG (s3918), siGRK5 (s6087), siLRRK1 (s36138), siSTYK1 (s30824) and siTPK1 (s25692). siRNA selection was based on WB experiments: each gene was knocked-down with two distinct siRNAs and the one producing the largest p.Phe508del-CFTR rescue was selected. The negative control siRNA was Neg1.

Preliminary control experiments were performed on cells expressing wt-CFTR. Cells grown on cover slips were mounted in a perfused bath on the stage of an inverted microscope (IM35, Zeiss) and kept at 37°C. The bath was perfused continuously with Ringer solution (mM: NaCl 145, KH_2PO_4 0.4, K_2HPO_4 1.6, D-glucose 5, $MgCl_2$ 1, Ca-gluconate 1.3, pH 7.4) containing 50 nM TRAM-34 at about 8 ml/min. Patch-clamp experiments were performed in the fast whole-cell configuration. Patch pipettes had an input resistance of 2–4 MΩ, and whole cell currents were corrected for serial resistance. Patch pipettes were filled with an intracellular like solution containing (mM) KCl 30, K-gluconate 95, NaH_2PO_4 1.2, Na_2HPO_4 4.8, EGTA 1, Ca-gluconate 0.758, $MgCl_2$ 1.034, D-glucose 5, ATP 3. pH was 7.2, the Ca^{2+} activity was 0.1 µM. According to the protocol we have previously established[75], the patch pipette is slightly hypotonic (270 mosmol/l when compared to the extracellular bath solution, which is 290 mosmol/l. Currents were recorded using a patch clamp amplifier (EPC 7, List Medical Electronics, Darmstadt, Germany), the LIH1600 interface and PULSE software (HEKA, Lambrecht, Germany) as well as Chart software (AD Instruments, Spechbach, Germany). In regular intervals, membrane voltages (Vc) were clamped in steps of 20 mV from -100 to +100 mV from holding potential of -100 mV. CFTR was stimulated with 25 µM Genistein and 2 µM Forskolin (Gen/Fsk). Current density was calculated by dividing whole-cell currents by cell capacitance. The calculated chloride equilibrium potential was -37.0 mV.

Ussing Chamber recordings

pHBE cells were treated with 3 µM VX-445 in combination with 5 µM VX-661 for 48h. DMSO or 500 nM 9j were added in the last 24h. CFTR function was assessed in Ussing Chamber as previously described by Awatade et al[67]. The transepithelial voltage (Vte) and transepithelial resistance (Rte) were recorded and used to calculate the equivalent short-circuit current (Isc-eq) using Ohm's law: Isc-eq = Vte/Rte. Experiments were performed by sequentially adding apically 20 µM amiloride, followed by 100 µM IBMX in combination with 2 µM Forskolin (Fsk), 10 µM VX-770, and 30 µM CFTRinh-172.

Quantitative RT-PCR

RNA was extracted (Trizol method—Invitrogen—or Macherey Nagel Nucleospin columns), quantified by Nanodrop spectrophotometry and digested with DNase I. Approximately 1 µg of total RNA was subjected to reverse transcription (RT) with random primers to produce cDNA (NZYTech, Lisboa, Portugal). cDNA was diluted to give a final reaction mixture concentration between 0.5 and 1.5 ng/µL. Each gene transcript was amplified in separate reactions by qRT-PCR using the SsoFast EvaGreen system (Bio-Rad, Hercules, CA), with primer sequences obtained from the Harvard primerbank (https://pga.mgh.harvard.edu/primerbank, **Dataset**

S1). Melt curves were checked to confirm amplification of single products, and negative controls were confirmed to be free of nonspecific amplification at 40 cycles. Products were quantified using the ΔΔCT method, normalized using as a reference gene either CAP-1 (adenylate cyclase associated protein 1) or ACTB (β actin). The correct size of amplification products was verified by agarose gel electrophoresis.

Bioinformatic analyses

The scores from different CFTR variants obtained at the ERQC classification screen were compared with a heatmap coupled to hierarchical clustering, using a custom R script relying on the heatmaply package [76]. Data was kept in the Z-score scale and was not further normalized.

Statistical overrepresentation tests of the Gene Ontology annotation were performed on Panther (http://www.pantherdb.org) [77], with Bonferroni correction. The complete term database was used.

Intersections of current data with other CFTR-related datasets

The following datasets were considered: the primary and confirmed hit genes enhancing p.Phe508del-CFTR traffic (this study), p.Phe508del-CFTR interactome in HBE41o$^-$ cells [28], p.Phe508del-CFTR interactome in CFBE 410- cells [29,30], genes whose silencing significantly rescued p.Phe508del-CFTR activity [31], candidate modifier genes of CF lung disease [32], ENaC activating genes in A549 cells [33] and protein secretion machinery in HeLa cells [34]. Gene identification was based on Uniprot IDs.

Chemistry General Remarks

All solvents were purchased from commercial sources and were dried according to standard methods. All chemicals and starting materials (2-oxoindoline-5-carboxylic acid, (S)-1-phenylethan-1-amine, HATU, 3,5-dimethyl-4-nitro-1H-pyrrole-2-carbaldehyde, bromoacetic acid, DIPEA, piperidine and zinc powder) were purchased from Fluorochem and Sigma-Aldrich. Reactions were monitored by TLC using 0.25 mm silica gel 60 F_{254} TLC plates purchased from Merck. Spots were visualized under ultraviolet light (254 nm).

^{1}H, ^{13}C APT NMR spectra were acquired on a Bruker Avance 400 spectrometer equipped with a 5 mm QNP probe operating at 400.16 MHz and 100.61 MHz for ^{1}H and ^{13}C respectively, at 293K. Spectra of all compounds were recorded using DMSO-d_6 (99.9%; Eurisotop, UK). Spectroscopic data of all compounds was matched with the one previously reported [45]. High-Resolution-Mass Spectrometry (HR-MS) and low-resolution Mass Spectrometry (MS) spectra were performed on an Impact II QTOF (Bruker, Bremen, Germany) mass spectrometer with an electrospray ionization source (ESI). The method consisted of direct infusions with MS/MS scans, in the positive and negative modes

9g Synthetic Procedure

The (R,Z)-3-((4-(2-bromoacetamido)-3,5-dimethyl-1H-pyrrol-2-yl)-methylene)-2-oxo-N-(1-phenylethyl)indoline-5-carboxamide (9g, **5**) was synthesized employing slight modifications of the Rowlands et al. method [45]. In the second step, reaction time was cut in half and the yield increased to 87%. In the last step of the synthesis, the reported coupling agent was DMTMM with a yield of 39%, while we used HATU which afforded the final compound (**5**) in 55% yield (Scheme 1). The NMR spectra of the final product is shown in **Fig. S10**.

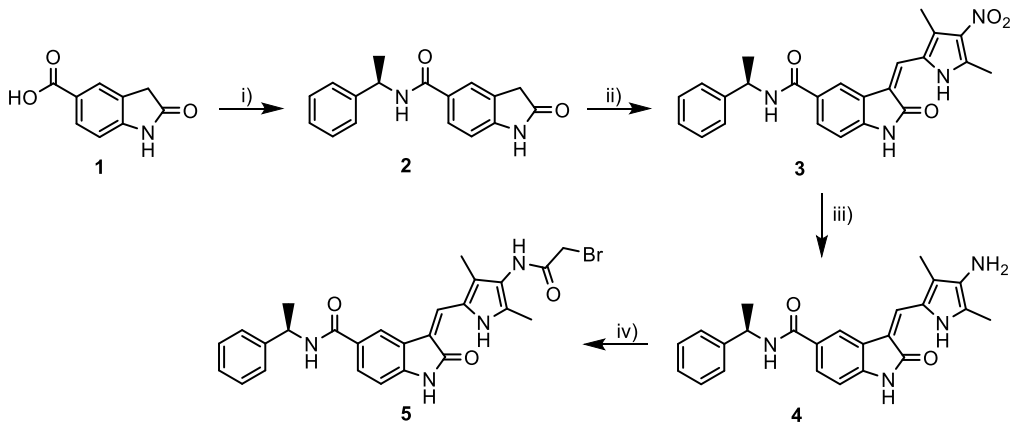

Scheme 1 – i) (S)-1-phenylethylamine, HATU, DIPEA, DMF, rt, overnight, 84%; ii) 3,5-dimethyl-4-nitro-1H-pyrrole-2-carbaldehyde, piperidine, EtOH, 95°C, 2h, 87%; iii) zinc powder, AcOH, EtOAc, EtOH, 50°C, 2h, 79%; iv) bromoacetic acid, HATU, DIPEA, DMF, rt, overnight, 55%.

Data and code availability

CellProfiler project files, shading correction files and output files are available at https://doi.org/10.5281/zenodo.6617740. HCS data analysis scripts are available as reproducible R markdown files at the same URL. Interactome processing code is available at https://doi.org/10.5281/zenodo.6646236.

QUANTIFICATION AND STATISTICAL ANALYSIS

Results are presented as mean or median ± SD or SEM, with the number of biological replicates indicated in the figure, figure legend or accompanying supplementary dataset. Hypothesis testing was performed by unpaired two-tailed Student's *t*-tests (pairwise comparison), one-way ANOVA followed by Dunnett's post-hoc test (multiple comparisons) or one sample *t*-test, as implemented in the GraphPad Prism software. Correlation analysis was performed on R. 0.05 significance was required.

Supplemental Figure Legends

Figure S1. High-content screening strategy, related to Figures 1, 2 and Methods. (A) Topology of the mCherry-Flag-CFTR traffic reporter, expressed in CFBE cells under the control of a Tet-inducible promoter. PM CFTR can be immunolabeled in unpermeabilized cells. (B) Workflow of the CFTR traffic assay for siRNA screening. (C) Image quantification algorithm, showing the mCherry-Flag-wt-CFTR construct. Initially, nuclei are segmented and used as seeds to estimate the cytoplasm location. Then, cells touching the image border, missing CFTR expression or containing apoptotic nuclei or saturated pixels are excluded from analysis. Fluorescence is quantified in approved cells, in the mCherry (total CFTR expression) or Flag(A647) (PM CFTR) channels. Data from images which are either out-of-focus or contain few cells are discarded (not shown). (D) Z-score calculation in the primary screen. The reference value for Z-score calculation is provided by the 5×5 well neighbourhood, when available. (E) Z-score calculation in the secondary, classification and 9g screens: classical control-based Z-score.

Figure S2. Primary screen hit pathways, related to Figure 1. Panther was used to assess the overrepresentation of GO annotation terms of enhancer genes hits: (A) molecular function, (B) biological process, (C) cellular compartment. Panther was used to assess the overrepresentation of GO annotation terms of inhibitor genes hits: (D) molecular function, (E) biological process, (F) cellular compartment.

Figure S3. Western blot analysis of the KD of primary screen genes which were not confirmed in the secondary rescreening step, related to Figure 1 and 3. CFBE cells overexpressing p.Phe508del-CFTR were transfected with siRNAs targeting 18 high-scoring primary hits which were not confirmed in the HT microscopy assay. (A) CFTR detection in a WB membrane. wt-CFTR was included for reference. The localization of core glycosylated (band B) and fully glycosylated CFTR (band C) are shown. Quantification of band B (B), band C (C) as well as p.Phe508del-CFTR processing efficiency [C/(B+C)] (D). The baseline readout, given by cells treated with the Neg1 siRNA, is given as a dotted line. ´*´ indicates statistical significance from Neg1-treated ($p<0.05$, one-way ANOVA followed by Dunnett's post-hoc test, n=3 biological replicates). Plot values are mean ± SD. Gel lanes were reordered and juxtaposed for presentation consistency and clarity.

Figure S4. Mechanistic analysis of the 53 confirmed hit genes, related to Results ("Classification of traffic regulators"). (A) Hierarchical clustering of the classification screen results for the 53 genes whose KD was confirmed to rescue p.Phe508del-CFTR traffic (HCS) or processing (WB). Each line in the y-axis is a single siRNA. The rows dendrogram highlights the 5 clusters mentioned in the results. For simplicity, single letter amino acid codes are used. (B) Number of common hit genes for the several CFTR variants. Legacy variant names are used

for simplicity. (C) Simplified representation of A, showing only hit kinases. (D) Co-occurrence of genes in the p.Phe508del-CFTR traffic screens (this study) and other CFTR-related datasets: p.Phe508del-CFTR interactome in HBE410- cells (Pankow et al., 2015), p.Phe508del-CFTR interactome in CFBE41o- cells (Canato et al., 2018; Reilly et al., 2017), genes whose silencing significantly rescued p.Phe508del-CFTR activity (Tomati et al., 2018), candidate modifier genes of CF lung disease (Dang et al., 2020), ENaC activating genes in A549 cells (Almaça et al., 2013) and protein secretion machinery in HeLa cells (Simpson et al., 2012). For this study, the outer track represents the primary screen hits and the inner track represents the subset of 35 HCS confirmed genes. Each gene is represented as a line color coded for the Z-score. Inter-dataset comparisons were performed based on Uniprot IDs. Genes for which an updated Uniprot ID could not be found were discarded, explaining the discrepancy in the gene counts in the original publications and this figure. Common genes in published datasets are linked by thin gray arcs in the center of the plot. Primary screen hits are linked by thin dark red arcs. Hit genes conformed by HCS or WB are linked by thin bright red arcs. Hit kinase genes are linked by thick bright red arcs. Selected gene names are shown in corresponding red tones. GRK5 (an ENaC activating gene) is the only kinase reported in another study.

Figure S5. Whole cell currents measured in CFBE cell expressing wt-CFTR as a function of the Cl^- concentration distribution, related to Figure 6. (A) Our patch clamp experiments were performed under physiological conditions: 37 °C, perfused experimental bath, and in the presence of an intracellular (pipette) ion composition that come close to cellular conditions, with Ringer solution in the bath (about 145 mM Cl^-) and a cytosolic-like ion composition in the patch pipette filling solution (containing (mM) KCl 30, K-gluconate 95, NaH_2PO_4 1.2, Na_2HPO_4 4.8, EGTA 1, Ca-gluconate 0.758, $MgCl_2$ 1.034, D-glucose 5, ATP 3. pH was 7.2, and Ca^{2+} activity 0.1 µM). Under these conditions there is a Cl^- gradient from outside 145 mM to inside (patch pipette) 35 mM and currents are outwardly rectifying when CFTR is activated through stimulation with forskolin (2 µM) and genistein (25 µM). **(B)** Under symmetric Cl^- conditions, the activated CFTR current is symmetric and linear (no longer outwardly rectifying). Moreover, in the presence of additional $CFTR_{inh}172$ (20 µM), the activated current is strongly (95 %) inhibited under either condition, indicating activation of CFTR currents, with little contribution of other currents. Values are mean ± SD. Numbers within parenthesis are the replicate count.

Figure S6. Western blot analysis of the additivity of CFTR folding correctors on the glycosylation of DD/AA-CFTR and p.Phe508del-CFTR traffic revertants, related to Results ("Classification of traffic regulators"). WB analysis of CFBE cells expressing p.Phe508del revertants p.Phe508del-p.Gly550Glu-CFTR (A), p.Phe508del-p.Arg1070Trp-CFTR (B), p.Phe508del-4RK-CFTR (C) or the DD/AA-CFTR variant (D). The quantification of CFTR's band B, C and processing [C/(B+C)] is shown. Symbols indicate statistic difference versus Neg1/DMSO- (´*´), Neg1/VX-445 (´#´) or Neg1/VX-664/VX-445-treated cells (´‡´) ($p<0.05$, one-way ANOVA followed by Dunnett's post-hoc test. n=4 biological replicates, except for p.Phe508del-4RK-CFTR treated with VX-445, n=3). Plot values are mean ± SD. Gel lanes were reordered and juxtaposed for presentation consistency and clarity.

Figure S7. Western blot analysis of the additivity of CFTR folding correctors on the glycosylation of selected non-p.Phe508del CFTR class II variants, related to Results ("Classification of traffic regulators"). CFBE cells overexpressing p.Arg560Ser- (A), p.Gly85Glu- (B) or p.Asn1303Lys-CFTR (C) were transfected with Neg1 or siRNAs targeting LRRK1, STYK1, TPK1, DGKG or GRK5, together with DMSO or a VX-661 (5 μM) plus VX-445 (3 μM) combination and the CFTR glycosylation pattern was analysed by WB. Representative membranes and quantification of band C, band B and processing efficiency, all normalized to the calnexin (CNX) loading control. $p > 0.05$ (unpaired *t*-test, VX-661/VX-445 versus corresponding DMSO, n=3 biological replicates). Plot values are mean ± SD. Gel lanes were reordered and juxtaposed for presentation consistency and clarity.

Figure S8. Inhibition of GRK5 with CCG-273441 (also known as 9j) rescues p.Phe508del-CFTR processing and ionic conductance, related to Figure 8. (A) 9j is a structural analogue of 9g, with equivalent chemical and biochemical properties, available from a quality-controlled commercial source (see methods) and with stability suitable for several month-long rounds of assays. **(B)** Dose-response curve and EC_{50} for CFBE p.Phe508del-CFTR cells grown in the presence of 9j. Obtained with the resazurin reduction assay (n=3 biological replicates). **(C)** CFBE cells expressing p.Phe508del-CFTR were incubated with VX-661 (5 μM) and VX-445 (3 μM) in the absence or presence of 9j, for 24 or 48 h. Densitometric analysis revealed a significant rescue of band C after 48 h exposure to 300 nM 9j **(D)**. Given the concomitant increase in band B **(E)** without change in processing efficiency **(F)** (one sample *t*-test), we surmise that the mechanism of action is increasing the CFTR steady state concentration and, thereby, exposing more molecules to folding correction by modulators. Replicate numbers are shown above each bar. **(G)** Representative HS-YFP quenching curves obtained with CFBE cells co-expressing p.Phe508del-CFTR and HS-YFP after 48h treatment with DMSO, and VX-661 plus VX-445 alone and in combination with 9j. The arrow indicates iodide addition. Exponential fits and dashed lines (during the 2-second iodide addition period) were added to guide the eye. **(H)** CFTR activity quantification based on the HS-YFP quenching rate normalized to VX-661 and VX-445 combination. One-way ANOVA followed by Dunnett's post-hoc test, n=4 biological replicates. *, $p < 0.05$; **, $p < 0.01$; ***, $p < 0.001$. All values are mean ± SD.

Figure S9. Expression of CFTR and GRK5 mRNA in CFBE cells, related to Figures 3 and 7. (A) RT-PCR quantification of p.Phe508del-CFTR mRNA following knock-down of the 14 best secondary screen hits (LIN9 through KIF17), as well as DGKG, GRK5 and STYK1. This set of siRNAs targets all 5 hit kinases. (LRRK1, TPK1, DGKG, GRK5 and STYK1. Results are ΔΔCT versus the Neg1 negative control, expressed as fold change. Significant CFTR mRNA expression variation was only found when knocking-down KIF17, a borderline $p=0.044$ in one-way ANOVA followed by Dunnett's post-hoc test (n=3 biological replicates)s. **(B)** RT-PCR quantification of GRK5 mRNA I cells expressing wt- or p.Phe508del-CFTR following GRK5 inhibition (9g 1μM), in the presence or absence of the VX-770 plus VX-661 plus VX-445 combination (ETI). n = 3-6 biological replicates. No statistically significant differences were observed. All plot values are mean ± SD,.

Figure S10. NMR spectra for compound 9g, related to Methods ("9g Synthetic Procedure"). (A) Structure and atom numbering for compound 9g. **(B)** ^{1}H NMR (400 MHz, DMSO-d_6) d 13.52 (s, 1H, H_{18}), 11.10 (s, 1H, H_1), 9.63 (s, 1H,H_{24}), 8.62 (d, *J* = 7.9 Hz, 1H, H_9), 8.22 (brs, 1H, H_4), 7.69 (dd, *J* = 8.1, 1.3 Hz, 1H, H_6), 7.65 (s, 1H, H_{16}), 7.41 (d, *J* = 7.4 Hz, 2H, H_{12}), 7.33 (t, *J* = 7.6 Hz, 2H, H_{13}), 7.23 (d, *J* = 7.4 Hz, 1H, H_{14}), 6.94 (d, *J* = 8.1 Hz, 1H, H_7), 5.19 (p, *J* = 7.2 Hz, 1H, H_{10}), 4.03 (s, 2H, H_{26}), 2.21 (s, 3H, H_{22}), 2.20 (s, 3H, H_{23}), 1.51 (d, *J* = 7.1 Hz, 3H, H_{15}). **(C)**^{13}C NMR (101 MHz, DMSO-d_6) d 169.74 (C_2), 166.12 (C_{25}), 165.48 (C_8), 144.90 (C_{11}), 141.18 (C_{7a}), 131.54 (C_{19}), 128.22 (C_{3a}), 128.10 (C_{13}), 127.41 (C_6), 126.44 (C_{14}), 126.00 (C_{12}), 124.99 (C_{17}), 124.64 (C_{21}), 124.31 (C_5), 123.48 (C_{16}), 121.12 (C_3), 118.87 (C_4), 112.49 (C_{20}), 108.99 (C_7), 48.33 (C_{10}), 29.21 (C_{26}),22.19 (C_{15}), 11.15 (C_{22}), 9.33 (C_{23}).

Supplemental Table Legends

Table S1. Confirmed hit genes and scores (secondary screen), related to Figures 1, 2 and Dataset S3. We defined as confirmed the genes which were hits with 2 siRNAs, considering the primary and secondary screens. The decision took was based on PM CFTR Z-scores. The table presents the scores obtained for every hit siRNA targeting the 35 confirmed genes. The table is ranked by the average PM Z-score of the 2 siRNAs.

Table S2. Effect of top hit genes on p.Phe508del-CFTR processing assessed by WB, related to Figure 3 and S3. Quantification of the WB data obtained when performing KD of confirmed screen hits and selected primary screen siRNAs which did not meet the hit threshold. The table indicates if the gene was part of the confirmed hits, the Ambion Silener Select siRNA catalog number as well as the quantification of p.Phe508del-CFTR band C, B and CFTR processing [C/(B+C)]. ´*´ indicates statistical significance (sig) from cells treated with the non-targeting Neg1 siRNA ($p<0.05$, one-way ANOVA followed by Dunnett's post-hoc test, n=3). n.a: not available, not performed.

Table S3. Specificity analysis of the classification screen, related to Figure 1 and S4 and Dataset S6. Gene KDs which significantly increased PM delivery of the CFTR variants used in the classification screen (hits, $Z > +1$) which were not hits in p.Phe508del-CFTR. The table is sorted alphabetically, and row numbers are shown.

Table S4. ERQC analysis of the classification screen, related to Figure 1 and S4 and Dataset S6. Gene KDs which significantly increased PM delivery of p.Phe508del-CFTR ($Z > +1$) but inhibited PM delivery of the indicated variants ($Z < -1$). The table is sorted alphabetically, and row numbers are shown.

Table S5. Knock-down efficiency of hit kinase genes, related to Figure 4 and 6. CFBE cells were reverse transfected with Ambion Silencer Select siRNAs, either a non-targeting sequence (Neg1) or siRNAs targeting each kinase: si3918 (DGKG), s36138 (LRRK1), s6087 (GRK5), s25692 (TPK1) and s30824 (STYK1). The expression of each gene was quantified through RT-PCR (ΔΔCT versus β-actin) and expressed as the normalized fold change relatively to the corresponding Neg1 treatment. The table shows the mean ± SD quantification, as well as the p-value (two-tailed unpaired Student's *t*-test, considering equal variance across samples). * indicates $p < 0.05$.

Supplemental Dataset Legends

Dataset S1. Primary screen scoring and hit genes.

Dataset S2. Gene Ontology (GO) overrepresentation tests for primary screen gene hits.

Dataset S3. Secondary screen scoring and hit genes.

Dataset S4. RT-PCR results for the 53 genes which were assayed in Western blot experiments. We analyzed the 35 confirmed hit genes (secondary screen) and 18 additional genes selected among the siRNAs which scored slightly below the hit threshold in the confirmation screen. CT values for expression in control lung tissue and CFBE cells overexpressing wt-CFTR. All genes amplified a product with single melt peak. The sequences of the primers used for amplification are shown.

Dataset S5. Scoring of the functional assessment by the HS-YFP fluorescence quenching assay for the 53 confirmed hit genes KDs.

Dataset S6. Classification screen scoring of the genes in the secondary siRNA library for their effects at ERQC checkpoints. Quantification for the following CFTR variants: wt, p.Phe508del-4RK-CFTR, p.Phe508del-p.Gly550Glu-CFTR, p.Phe508del-p.Arg1070Trp-CFTR, DD/AA-CFTR.

References

1. Riordan, J.R., Rommens, J.M., Kerem, B., Alon, N., Rozmahel, R., Grzelczak, Z., Zielenski, J., Lok, S., Plavsic, N., Chou, J.L., and et al. (1989). Identification of the cystic fibrosis gene: cloning and characterization of complementary DNA. Science *245*, 1066-1073.

2. MacKenzie, T., Gifford, A.H., Sabadosa, K.A., Quinton, H.B., Knapp, E.A., Goss, C.H., and Marshall, B.C. (2014). Longevity of patients with cystic fibrosis in 2000 to 2010 and beyond: survival analysis of the Cystic Fibrosis Foundation patient registry. Ann Intern Med *161*, 233-241. 10.7326/M13-0636.

3. Guo, J., Garratt, A., and Hill, A. (2022). Worldwide rates of diagnosis and effective treatment for cystic fibrosis. Journal of Cystic Fibrosis *21*, 456-462. https://doi.org/10.1016/j.jcf.2022.01.009.

4. Rommens, J.M. (2022). Cystic Fibrosis Mutation Database. http://www.genet.sickkids.on.ca/cftr/.

5. Amaral, M.D. (2004). CFTR and chaperones: processing and degradation. J Mol Neurosci *23*, 41-48. 10.1385/JMN:23:1-2:041.

6. Dalemans, W., Barbry, P., Champigny, G., Jallat, S., Dott, K., Dreyer, D., Crystal, R.G., Pavirani, A., Lecocq, J.P., and Lazdunski, M. (1991). Altered chloride ion channel kinetics associated with the delta F508 cystic fibrosis mutation. Nature *354*, 526-528. 10.1038/354526a0.

7. Moniz, S., Sousa, M., Moraes, B.J., Mendes, A.I., Palma, M., Barreto, C., Fragata, J.I., Amaral, M.D., and Matos, P. (2013). HGF stimulation of Rac1 signaling enhances pharmacological correction of the most prevalent cystic fibrosis mutant F508del-CFTR. ACS Chem Biol *8*, 432-442. 10.1021/cb300484r.

8. Okiyoneda, T., Veit, G., Dekkers, J.F., Bagdany, M., Soya, N., Xu, H., Roldan, A., Verkman, A.S., Kurth, M., Simon, A., et al. (2013). Mechanism-based corrector combination restores DeltaF508-CFTR folding and function. Nat Chem Biol *9*, 444-454. 10.1038/nchembio.1253.

9. Denning, G.M., Anderson, M.P., Amara, J.F., Marshall, J., Smith, A.E., and Welsh, M.J. (1992). Processing of mutant cystic fibrosis transmembrane conductance regulator is temperature-sensitive. Nature *358*, 761-764. 10.1038/358761a0.

10. Taylor-Cousar, J.L., Munck, A., McKone, E.F., van der Ent, C.K., Moeller, A., Simard, C., Wang, L.T., Ingenito, E.P., McKee, C., Lu, Y., et al. (2017). Tezacaftor-Ivacaftor in Patients with Cystic Fibrosis Homozygous for Phe508del. N Engl J Med *377*, 2013-2023. 10.1056/NEJMoa1709846.

11. Middleton, P.G., Mall, M.A., Drevinek, P., Lands, L.C., McKone, E.F., Polineni, D., Ramsey, B.W., Taylor-Cousar, J.L., Tullis, E., Vermeulen, F., et al. (2019). Elexacaftor-Tezacaftor-Ivacaftor for Cystic Fibrosis with a Single Phe508del Allele. N Engl J Med *381*, 1809-1819. 10.1056/NEJMoa1908639.

12. He, L., Kota, P., Aleksandrov, A.A., Cui, L., Jensen, T., Dokholyan, N.V., and Riordan, J.R. (2013). Correctors of DeltaF508 CFTR restore global conformational maturation without thermally stabilizing the mutant protein. FASEB J *27*, 536-545. 10.1096/fj.12-216119.

13. Fiedorczuk, K., and Chen, J. (2022). Mechanism of CFTR correction by type I folding correctors. Cell *185*, 158-168.e111. 10.1016/j.cell.2021.12.009.

14. Farinha, C.M., King-Underwood, J., Sousa, M., Correia, A.R., Henriques, B.J., Roxo-Rosa, M., Da Paula, A.C., Williams, J., Hirst, S., Gomes, C.M., and Amaral, M.D. (2013). Revertants, Low Temperature, and Correctors Reveal the Mechanism of F508del-CFTR Rescue by VX-809 and Suggest Multiple Agents for Full Correction. Chem Biol *20*, 943-955. 10.1016/j.chembiol.2013.06.004.

15. Baatallah, N., Elbahnsi, A., Mornon, J.P., Chevalier, B., Pranke, I., Servel, N., Zelli, R., Décout, J.L., Edelman, A., Sermet-Gaudelus, I., et al. (2021). Pharmacological chaperones improve intra-domain stability and inter-domain assembly via distinct binding sites to rescue misfolded CFTR. Cell Mol Life Sci *78*, 7813-7829. 10.1007/s00018-021-03994-5.

16. Farinha, C.M., and Amaral, M.D. (2005). Most F508del-CFTR is targeted to degradation at an early folding checkpoint and independently of calnexin. Mol Cell Biol *25*, 5242-5252. 10.1128/MCB.25.12.5242-5252.2005.

17. Amaral, M.D., and Farinha, C.M. (2013). Rescuing mutant CFTR: a multi-task approach to a better outcome in treating cystic fibrosis. Curr Pharm Des *19*, 3497-3508. 10.2174/1381612811319999031 8.

18. Amaral, M.D. (2021). How to determine the mechanism of action of CFTR modulator compounds: A gateway to theranostics. Eur J Med Chem *210*, 112989. 10.1016/j.ejmech.2020.112989.

19. Yarwood, R., Hellicar, J., Woodman, P.G., and Lowe, M. (2020). Membrane trafficking in health and disease. Dis Model Mech *13*, dmm043448. 10.1242/dmm.043448.

20. Farinha, C.M., and Canato, S. (2017). From the endoplasmic reticulum to the plasma membrane: mechanisms of CFTR folding and trafficking. Cell Mol Life Sci *74*, 39-55. 10.1007/s00018-016-2387-7.

21. Younger, J.M., Chen, L., Ren, H.Y., Rosser, M.F., Turnbull, E.L., Fan, C.Y., Patterson, C., and Cyr, D.M. (2006). Sequential quality-control checkpoints triage misfolded cystic fibrosis transmembrane conductance regulator. Cell *126*, 571-582. 10.1016/j.cell.2006.06.041.

22. Nishimura, N., and Balch, W.E. (1997). A di-acidic signal required for selective export from the endoplasmic reticulum. Science *277*, 556-558.

23. Wang, X., Matteson, J., An, Y., Moyer, B., Yoo, J.S., Bannykh, S., Wilson, I.A., Riordan, J.R., and Balch, W.E. (2004). COPII-dependent export of cystic fibrosis transmembrane conductance regulator from the ER uses a di-acidic exit code. J Cell Biol *167*, 65-74. 10.1083/jcb.200401035.

24. Teem, J.L., Berger, H.A., Ostedgaard, L.S., Rich, D.P., Tsui, L.C., and Welsh, M.J. (1993). Identification of revertants for the cystic fibrosis delta F508 mutation using STE6-CFTR chimeras in yeast. Cell *73*, 335-346. 10.1016/0092-8674(93)90233-g.

25. Dörk, T., Wulbrand, U., Richter, T., Neumann, T., Wolfes, H., Wulf, B., Maass, G., and Tümmler, B. (1991). Cystic fibrosis with three mutations in the cystic fibrosis transmembrane conductance regulator gene. Hum Genet *87*, 441-446. 10.1007/bf00197165.

26. Botelho, H.M., Uliyakina, I., Awatade, N.T., Proenca, M.C., Tischer, C., Sirianant, L., Kunzelmann, K., Pepperkok, R., and Amaral, M.D. (2015). Protein traffic disorders: an effective high-throughput fluorescence microscopy pipeline for drug discovery. Sci Rep *5*, 9038. 10.1038/srep09038.

27. Amaral, M.D., Farinha, C.M., Matos, P., and Botelho, H.M. (2016). Investigating Alternative Transport of Integral Plasma Membrane Proteins from the ER to the Golgi: Lessons from the Cystic Fibrosis Transmembrane Conductance Regulator (CFTR). Methods Mol Biol *1459*, 105-126. 10.1007/978-1-4939-3804-9_7.

28. Pankow, S., Bamberger, C., Calzolari, D., Martínez-Bartolomé, S., Lavallée-Adam, M., Balch, W.E., and Yates, J.R., 3rd (2015). ΔF508 CFTR interactome remodelling promotes rescue of cystic fibrosis. Nature *528*, 510-516. 10.1038/nature15729.

29. Canato, S., Santos, J.D., Carvalho, A.S., Aloria, K., Amaral, M.D., Matthiesen, R., Falcao, A.O., and Farinha, C.M. (2018). Proteomic interaction profiling reveals KIFC1 as a factor involved in early targeting of F508del-CFTR to degradation. Cell Mol Life Sci *75*, 4495-4509. 10.1007/s00018-018-2896-7.

30. Reilly, R., Mroz, M.S., Dempsey, E., Wynne, K., Keely, S.J., McKone, E.F., Hiebel, C., Behl, C., and Coppinger, J.A. (2017). Targeting the PI3K/Akt/mTOR signalling pathway in Cystic Fibrosis. Sci Rep *7*, 7642. 10.1038/s41598-017-06588-z.

31. Tomati, V., Pesce, E., Caci, E., Sondo, E., Scudieri, P., Marini, M., Amato, F., Castaldo, G., Ravazzolo, R., Galietta, L.J.V., and Pedemonte, N. (2018). High-throughput screening identifies FAU protein as a regulator of mutant cystic fibrosis transmembrane conductance regulator channel. J Biol Chem *293*, 1203-1217. 10.1074/jbc.M117.816595.

32. Dang, H., Polineni, D., Pace, R.G., Stonebraker, J.R., Corvol, H., Cutting, G.R., Drumm, M.L., Strug, L.J., O'Neal, W.K., and Knowles, M.R. (2020). Mining GWAS and eQTL data for CF lung disease modifiers by gene expression imputation. PLoS One *15*, e0239189. 10.1371/journal.pone.0239189.

33. Almaça, J., Faria, D., Sousa, M., Uliyakina, I., Conrad, C., Sirianant, L., Clarke, L.A., Martins, J.P., Santos, M., Hériché, J.-K., et al. (2013). High-content siRNA screen reveals global ENaC regulators and potential cystic fibrosis therapy targets. Cell *154*, 1390-1400. 10.1016/j.cell.2013.08.045.

34. Simpson, J.C., Joggerst, B., Laketa, V., Verissimo, F., Cetin, C., Erfle, H., Bexiga, M.G., Singan, V.R., Heriche, J.K., Neumann, B., et al. (2012). Genome-wide RNAi screening identifies human proteins with a regulatory function in the early secretory pathway. Nat Cell Biol *14*, 764-774. 10.1038/ncb2510.

35. Lim, S.H., Snider, J., Birimberg-Schwartz, L., Ip, W., Serralha, J.C., Botelho, H.M., Lopes-Pacheco, M., Pinto, M.C., Moutaoufik, M.T., Zilocchi, M., et al. (2022). CFTR interactome mapping using the mammalian membrane two-hybrid high-throughput screening system. Mol Syst Biol *18*, e10629. 10.15252/msb.202110629.

36. Benedetto, R., Ousingsawat, J., Wanitchakool, P., Zhang, Y., Holtzman, M.J., Amaral, M., Rock, J.R., Schreiber, R., and Kunzelmann, K. (2017). Epithelial Chloride Transport by CFTR Requires TMEM16A. Sci Rep *7*, 12397. 10.1038/s41598-017-10910-0.

37. Lerias, J., Pinto, M., Benedetto, R., Schreiber, R., Amaral, M., Aureli, M., and Kunzelmann, K. (2018). Compartmentalized crosstalk of CFTR and TMEM16A (ANO1) through EPAC1 and ADCY1. Cell Signal *44*, 10-19. 10.1016/j.cellsig.2018.01.008.

38. Lérias, J.R., Pinto, M.C., Botelho, H.M., Awatade, N.T., Quaresma, M.C., Silva, I.A.L., Wanitchakool, P., Schreiber, R., Pepperkok, R., Kunzelmann, K., and Amaral, M.D. (2018). A novel microscopy-based assay identifies extended synaptotagmin-1 (ESYT1) as a positive regulator of anoctamin 1 traffic. Biochim Biophys Acta Mol Cell Res *1865*, 421-431. 10.1016/j.bbamcr.2017.11.009.

39. Pinto, M.C., Botelho, H.M., Silva, I.A.L., Railean, V., Neumann, B., Pepperkok, R., Schreiber, R., Kunzelmann, K., and Amaral, M.D. (2022). Systems Approaches to Unravel Molecular Function: High-content siRNA Screen Identifies TMEM16A Traffic Regulators as Potential Drug Targets for Cystic Fibrosis. J Mol Biol *434*, 167436. 10.1016/j.jmb.2021.167436.

40. Thibodeau, P.H., Richardson, J.M., 3rd, Wang, W., Millen, L., Watson, J., Mendoza, J.L., Du, K., Fischman, S., Senderowitz, H., Lukacs, G.L., et al. (2010). The cystic fibrosis-causing mutation deltaF508 affects multiple steps in cystic fibrosis transmembrane conductance regulator biogenesis. J Biol Chem *285*, 35825-35835. 10.1074/jbc.M110.131623.

41. Roxo-Rosa, M., Xu, Z., Schmidt, A., Neto, M., Cai, Z., Soares, C.M., Sheppard, D.N., and Amaral, M.D. (2006). Revertant mutants G550E and 4RK rescue cystic fibrosis mutants in the first nucleotide-binding domain of CFTR by different mechanisms. Proc Natl Acad Sci U S A *103*, 17891-17896. 10.1073/pnas.0608312103.

42. Pfleger, J., Gresham, K., and Koch, W.J. (2019). G protein-coupled receptor kinases as therapeutic targets in the heart. Nat Rev Cardiol *16*, 612-622. 10.1038/s41569-019-0220-3.

43. Naren, A.P., Cobb, B., Li, C., Roy, K., Nelson, D., Heda, G.D., Liao, J., Kirk, K.L., Sorscher, E.J., Hanrahan, J., and Clancy, J.P. (2003). A macromolecular complex of beta 2 adrenergic receptor, CFTR, and

ezrin/radixin/moesin-binding phosphoprotein 50 is regulated by PKA. Proc Natl Acad Sci U S A *100*, 342-346. 10.1073/pnas.0135434100.

44. Fredericks, Z.L., Pitcher, J.A., and Lefkowitz, R.J. (1996). Identification of the G protein-coupled receptor kinase phosphorylation sites in the human beta2-adrenergic receptor. J Biol Chem *271*, 13796-13803. 10.1074/jbc.271.23.13796.

45. Rowlands, R.A., Chen, Q., Bouley, R.A., Avramova, L.V., Tesmer, J.J.G., and White, A.D. (2021). Generation of Highly Selective, Potent, and Covalent G Protein-Coupled Receptor Kinase 5 Inhibitors. J Med Chem *64*, 566-585. 10.1021/acs.jmedchem.0c01522.

46. Caci, E., Caputo, A., Hinzpeter, A., Arous, N., Fanen, P., Sonawane, N., Verkman, A.S., Ravazzolo, R., Zegarra-Moran, O., and Galietta, Luis J.V. (2008). Evidence for direct CFTR inhibition by CFTRinh-172 based on Arg347 mutagenesis. Biochemical Journal *413*, 135-142. 10.1042/BJ20080029.

47. Gao, X., Yeh, H.-I., Yang, Z., Fan, C., Jiang, F., Howard, R.J., Lindahl, E., Kappes, J.C., and Hwang, T.-C. (2024). Allosteric inhibition of CFTR gating by CFTRinh-172 binding in the pore. Nature Communications *15*, 6668. 10.1038/s41467-024-50641-1.

48. Young, P.G., Levring, J., Fiedorczuk, K., Blanchard, S.C., and Chen, J. (2024). Structural basis for CFTR inhibition by CFTRinh-172. Proceedings of the National Academy of Sciences *121*, e2316675121. 10.1073/pnas.2316675121.

49. Neumann, B., Walter, T., Hériché, J.-K., Bulkescher, J., Erfle, H., Conrad, C., Rogers, P., Poser, I., Held, M., Liebel, U., et al. (2010). Phenotypic profiling of the human genome by time-lapse microscopy reveals cell division genes. Nature *464*, 721-727. 10.1038/nature08869.

50. Moore, P.J., and Tarran, R. (2018). The epithelial sodium channel (ENaC) as a therapeutic target for cystic fibrosis lung disease. Expert Opin Ther Targets *22*, 687-701. 10.1080/14728222.2018.1501361.

51. Shei, R.J., Peabody, J.E., Kaza, N., and Rowe, S.M. (2018). The epithelial sodium channel (ENaC) as a therapeutic target for cystic fibrosis. Curr Opin Pharmacol *43*, 152-165. 10.1016/j.coph.2018.09.007.

52. Chen, Y., Sonawane, A., Manda, R., Gadi, R.K., Tesmer, J.J.G., and Ghosh, A.K. (2024). Development of a new class of potent and highly selective G protein-coupled receptor kinase 5 inhibitors and structural insight from crystal structures of inhibitor complexes. European Journal of Medicinal Chemistry *264*, 115931. https://doi.org/10.1016/j.ejmech.2023.115931.

53. Cholon, D.M., Quinney, N.L., Fulcher, M.L., Esther, C.R., Jr., Das, J., Dokholyan, N.V., Randell, S.H., Boucher, R.C., and Gentzsch, M. (2014). Potentiator ivacaftor abrogates pharmacological correction of DeltaF508 CFTR in cystic fibrosis. Sci Transl Med *6*, 246ra296. 10.1126/scitranslmed.3008680.

54. Veit, G., Avramescu, R.G., Perdomo, D., Phuan, P.W., Bagdany, M., Apaja, P.M., Borot, F., Szollosi, D., Wu, Y.S., Finkbeiner, W.E., et al. (2014). Some gating potentiators, including VX-770, diminish ΔF508-CFTR functional expression. Sci Transl Med *6*, 246ra297. 10.1126/scitranslmed.3008889.

55. Keating, D., Marigowda, G., Burr, L., Daines, C., Mall, M.A., McKone, E.F., Ramsey, B.W., Rowe, S.M., Sass, L.A., Tullis, E., et al. (2018). VX-445-Tezacaftor-Ivacaftor in Patients with Cystic Fibrosis and One or Two Phe508del Alleles. N Engl J Med *379*, 1612-1620. 10.1056/NEJMoa1807120.

56. Traynham, C.J., Hullmann, J., and Koch, W.J. (2016). "Canonical and non-canonical actions of GRK5 in the heart". J Mol Cell Cardiol *92*, 196-202. 10.1016/j.yjmcc.2016.01.027.

57. Boccella, N., Paolillo, R., and Perrino, C. (2019). Epac1 inhibition as a novel cardioprotective strategy: lights and shadows on GRK5 canonical and non-canonical functions. Cardiovasc Res *115*, 1684-1686. 10.1093/cvr/cvz188.

58. Billington, C.K., Penn, R.B., and Hall, I.P. (2017). β(2) Agonists. Handb Exp Pharmacol *237*, 23-40. 10.1007/164_2016_64.

59. Winter, M.C., and Welsh, M.J. (1997). Stimulation of CFTR activity by its phosphorylated R domain. Nature *389*, 294-296. 10.1038/38514.

60. Lobo, M.J., Amaral, M.D., Zaccolo, M., and Farinha, C.M. (2016). EPAC1 activation by cAMP stabilizes CFTR at the membrane by promoting its interaction with NHERF1. J Cell Sci *129*, 2599-2612. 10.1242/jcs.185629.

61. Gurevich, E.V., Tesmer, J.J., Mushegian, A., and Gurevich, V.V. (2012). G protein-coupled receptor kinases: more than just kinases and not only for GPCRs. Pharmacol Ther *133*, 40-69. 10.1016/j.pharmthera.2011.08.001.

62. Sibley, D.R., Strasser, R.H., Caron, M.G., and Lefkowitz, R.J. (1985). Homologous desensitization of adenylate cyclase is associated with phosphorylation of the beta-adrenergic receptor. J Biol Chem *260*, 3883-3886.

63. Stadel, J.M., Rebar, R., and Crooke, S.T. (1987). Catecholamine-induced desensitization of adenylate cyclase coupled beta-adrenergic receptors in turkey erythrocytes: evidence for a two-step mechanism. Biochemistry *26*, 5861-5866. 10.1021/bi00392a042.

64. Lieu, M., and Koch, W.J. (2019). GRK2 and GRK5 as therapeutic targets and their role in maladaptive and pathological cardiac hypertrophy. Expert Opin Ther Targets *23*, 201-214. 10.1080/14728222.2019.1575363.

65. Hendrickx, J.O., van Gastel, J., Leysen, H., Santos-Otte, P., Premont, R.T., Martin, B., and Maudsley, S. (2018). GRK5 - A Functional Bridge Between Cardiovascular and Neurodegenerative Disorders. Front Pharmacol *9*, 1484. 10.3389/fphar.2018.01484.

66. Beyett, T.S., Fraley, A.E., Labudde, E., Patra, D., Coleman, R.C., Eguchi, A., Glukhova, A., Chen, Q., Williams, R.M., Koch, W.J., et al. (2019). Perturbation of the interactions of calmodulin with GRK5 using a natural product chemical probe. Proc Natl Acad Sci U S A *116*, 15895-15900. 10.1073/pnas.1818547116.

67. Awatade, N.T., Uliyakina, I., Farinha, C.M., Clarke, L.A., Mendes, K., Solé, A., Pastor, J., Ramos, M.M., and Amaral, M.D. (2015). Measurements of Functional Responses in Human Primary Lung Cells as a Basis for Personalized Therapy for Cystic Fibrosis. EBioMedicine *2*, 147-153. https://doi.org/10.1016/j.ebiom.2014.12.005.

68. Almaça, J., Dahimène, S., Appel, N., Conrad, C., Kunzelmann, K., Pepperkok, R., and Amaral, M.D. (2011). Functional genomics assays to study CFTR traffic and ENaC function. Methods Mol Biol *742*, 249-264. 10.1007/978-1-61779-120-8_15.

69. Sondo, E., Tomati, V., Caci, E., Esposito, A.I., Pfeffer, U., Pedemonte, N., and Galietta, L.J. (2011). Rescue of the mutant CFTR chloride channel by pharmacological correctors and low temperature analyzed by gene expression profiling. Am J Physiol Cell Physiol *301*, C872-885. 10.1152/ajpcell.00507.2010.

70. Bebok, Z., Collawn, J.F., Wakefield, J., Parker, W., Li, Y., Varga, K., Sorscher, E.J., and Clancy, J.P. (2005). Failure of cAMP agonists to activate rescued deltaF508 CFTR in CFBE41o- airway epithelial monolayers. J Physiol *569*, 601-615. 10.1113/jphysiol.2005.096669.

71. Pedemonte, N., Zegarra-Moran, O., and Galietta, L.J. (2011). High-throughput screening of libraries of compounds to identify CFTR modulators. Methods Mol Biol *741*, 13-21. 10.1007/978-1-61779-117-8_2.

72. Erfle, H., Neumann, B., Liebel, U., Rogers, P., Held, M., Walter, T., Ellenberg, J., and Pepperkok, R. (2007). Reverse transfection on cell arrays for high content screening microscopy. Nat Protoc *2*, 392-399. 10.1038/nprot.2006.483.

73. Hagemeijer, M.C., Vonk, A.M., Awatade, N.T., Silva, I.A.L., Tischer, C., Hilsenstein, V., Beekman, J.M., Amaral, M.D., and Botelho, H.M. (2021). An open-source high-content analysis workflow for CFTR function measurements using the forskolin-induced swelling assay. Bioinformatics *36*, 5686-5694. 10.1093/bioinformatics/btaa1073.

74. Carpenter, A.E., Jones, T.R., Lamprecht, M.R., Clarke, C., Kang, I.H., Friman, O., Guertin, D.A., Chang, J.H., Lindquist, R.A., Moffat, J., et al. (2006). CellProfiler: image analysis software for identifying and quantifying cell phenotypes. Genome Biol *7*, R100. 10.1186/gb-2006-7-10-r100.

75. Greger, R., and Kunzelmann, K. (1991). Simultaneous recording of the cell membrane potential and properties of the cell attached membrane of HT29 colon carcinoma and CF-PAC cells. Pflugers Arch *419*, 209-211. 10.1007/BF00373009.

76. Galili, T., O'Callaghan, A., Sidi, J., and Sievert, C. (2018). heatmaply: an R package for creating interactive cluster heatmaps for online publishing. Bioinformatics *34*, 1600-1602. 10.1093/bioinformatics/btx657.

77. Thomas, P.D., Campbell, M.J., Kejariwal, A., Mi, H., Karlak, B., Daverman, R., Diemer, K., Muruganujan, A., and Narechania, A. (2003). PANTHER: a library of protein families and subfamilies indexed by function. Genome Res *13*, 2129-2141. 10.1101/gr.772403.

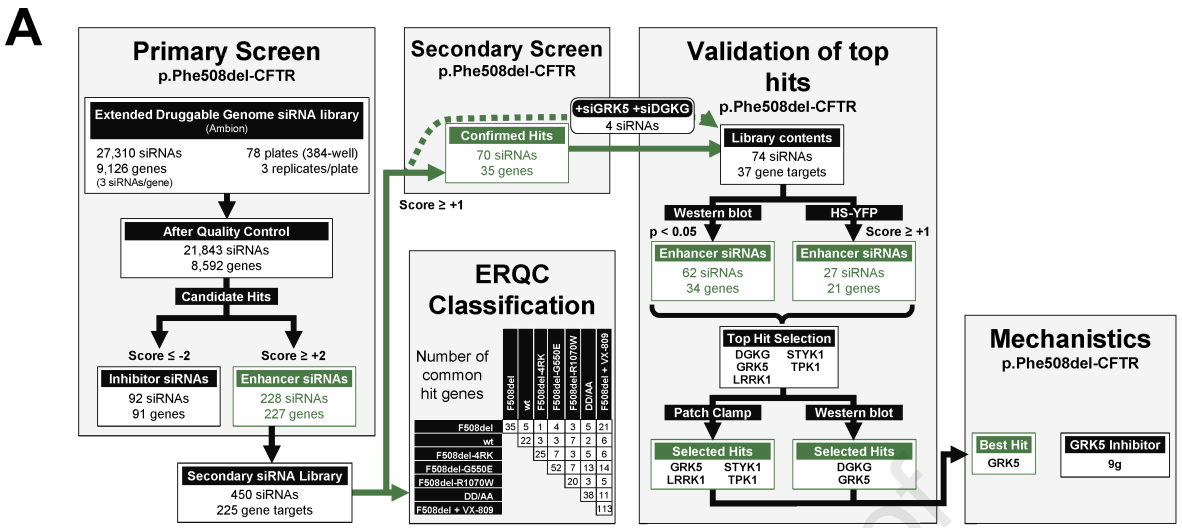

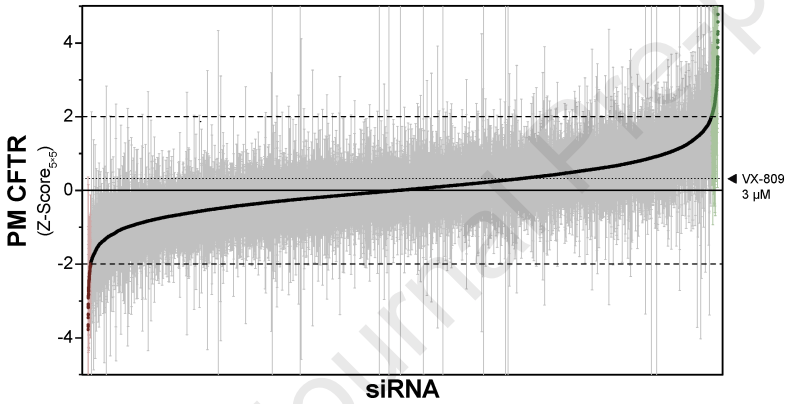

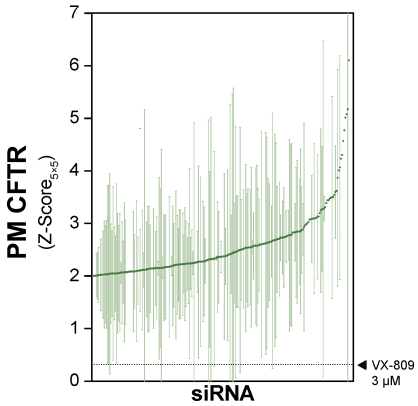

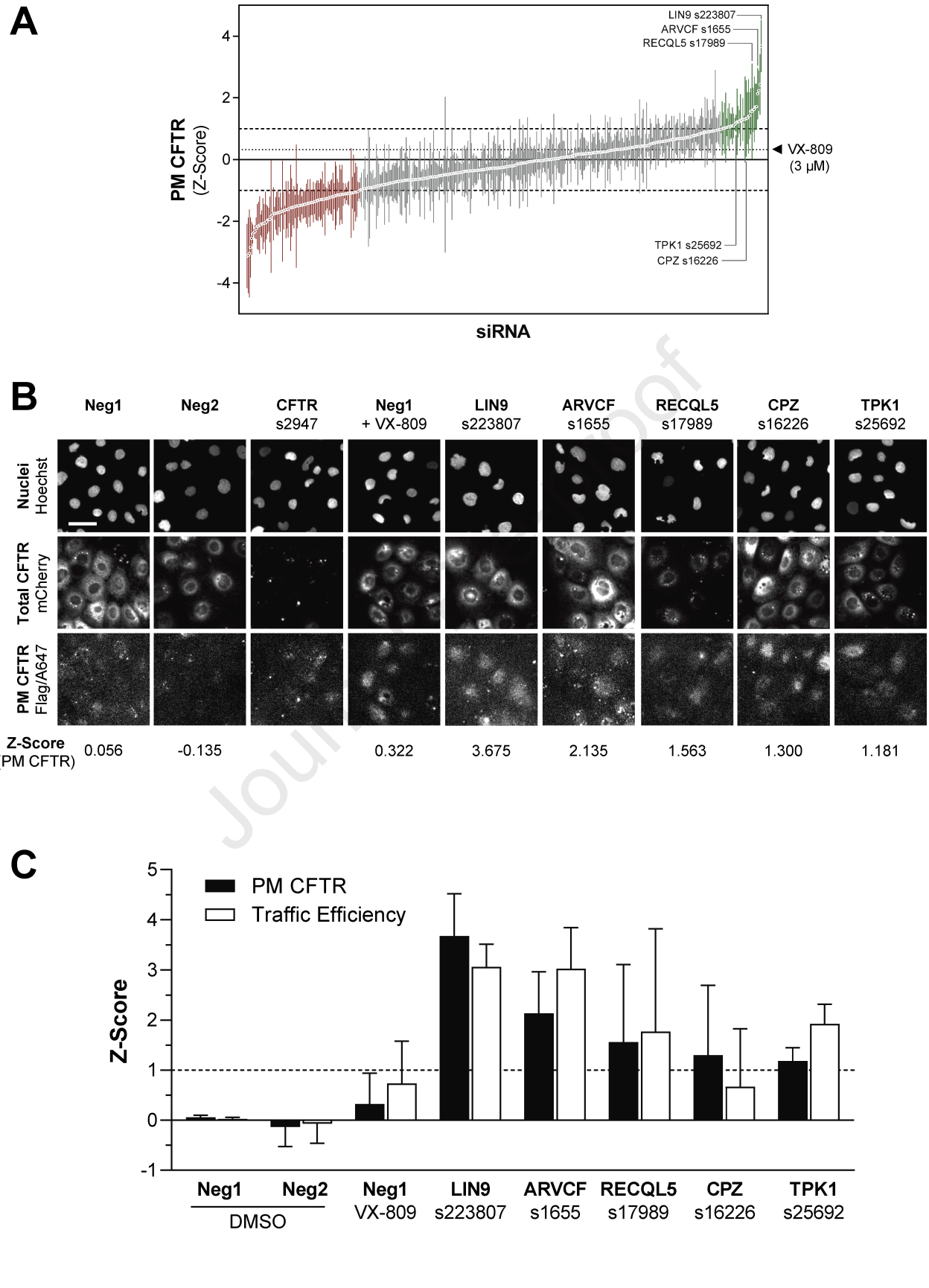
A
LIN9 s223807
ARVCF s1655
RECQL5 s17989
PM CFTR
(Z-Score)
VX-809
(3 μM)
TPK1 s25692
CPZ s16226
siRNA
B
Neg1
Neg2
CFTR
s2947
Neg1
+ VX-809
LIN9
s223807
ARVCF
s1655
RECQL5
s17989
CPZ
s16226
TPK1
s25692
Nuclei
Hoechst
Total CFTR
mCherry
PM CFTR
Flag/A647
Z-Score
(PM CFTR)
0.056
-0.135
0.322
3.675
2.135
1.563
1.300
1.181
C
PM CFTR
Traffic Efficiency
Z-Score
Neg1
Neg2
DMSO
Neg1
VX-809
LIN9
s223807
ARVCF
s1655
RECQL5
s17989
CPZ
s16226
TPK1
s25692

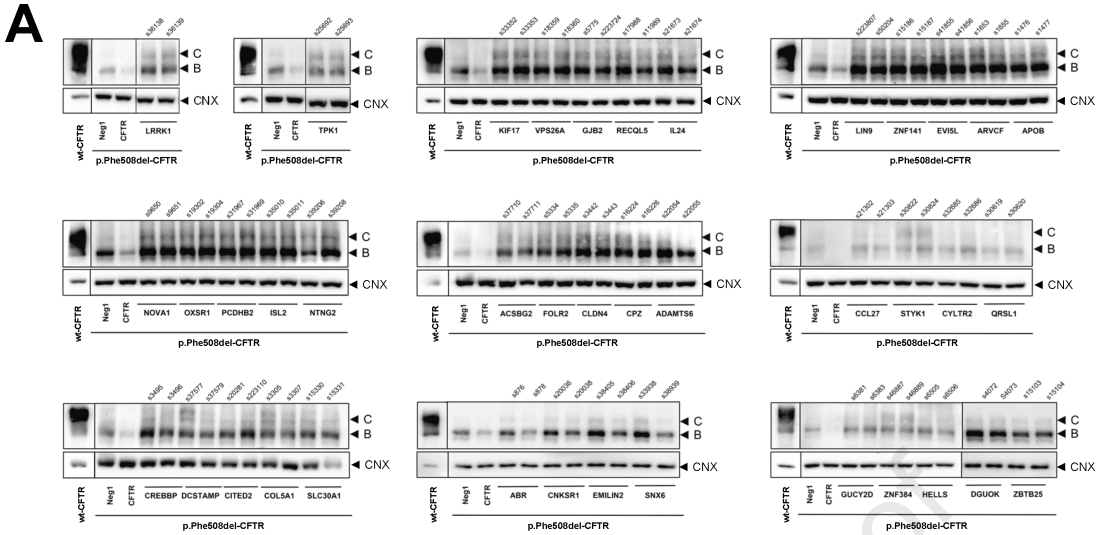
A
wt-CFTR
Neg1
CFTR
LRRK1
TPK1
KIF17
VPS26A
GJB2
RECQL5
IL24
LIN9
ZNF141
EVI5L
ARVCF
APOB
NOVA1
OXSR1
PCDHB2
ISL2
NTNG2
CLDN4
CPZ
ADAMTS6
CCL27
STYK1
CYLTR2
QRSL1
CREBBP
DCSTAMP
CITED2
COL5A1
SLC30A1
ABR
CNKSR1
EMILIN2
SNX6
GUCY2D
ZNF384
HELLS
DGUOK
ZBTB25
C
B
CNX
p.Phe508del-CFTR

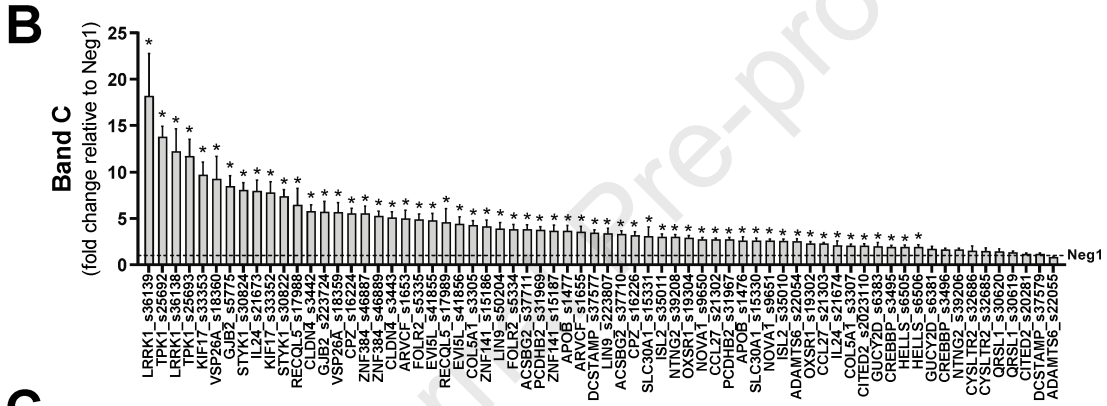
B
Band C
(fold change relative to Neg1)
Neg1

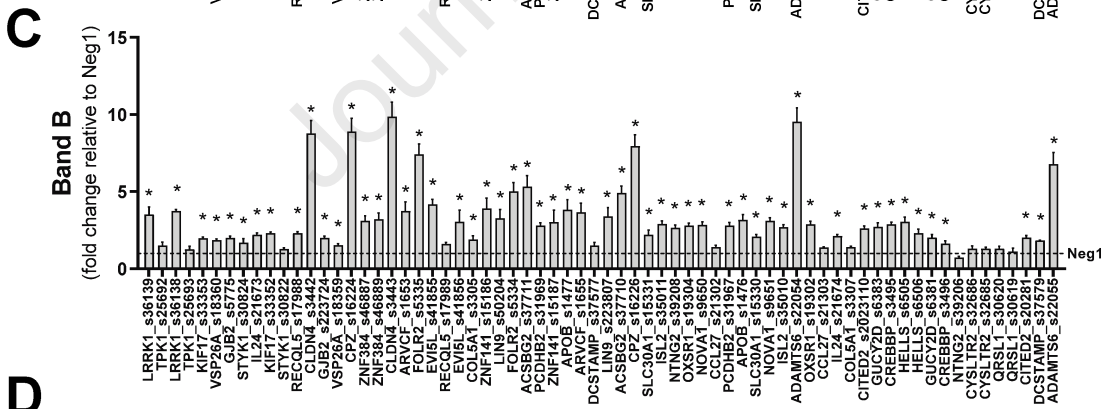
C
Band B
(fold change relative to Neg1)
Neg1

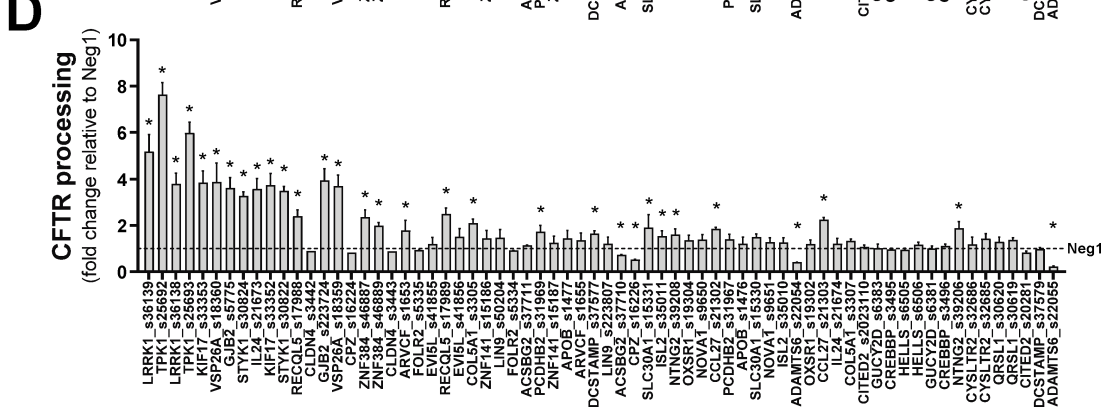
D
CFTR processing
(fold change relative to Neg1)
Neg1

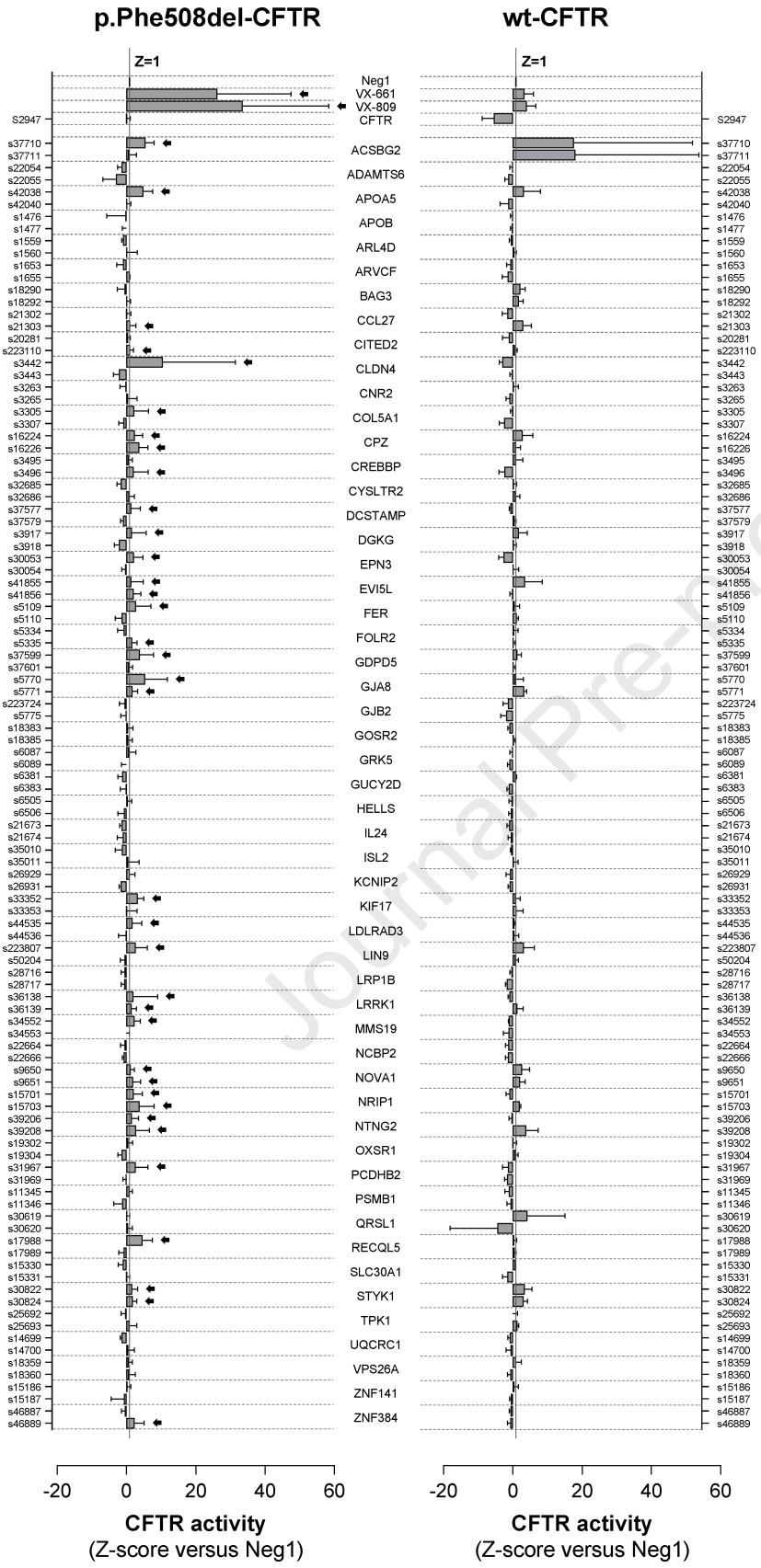

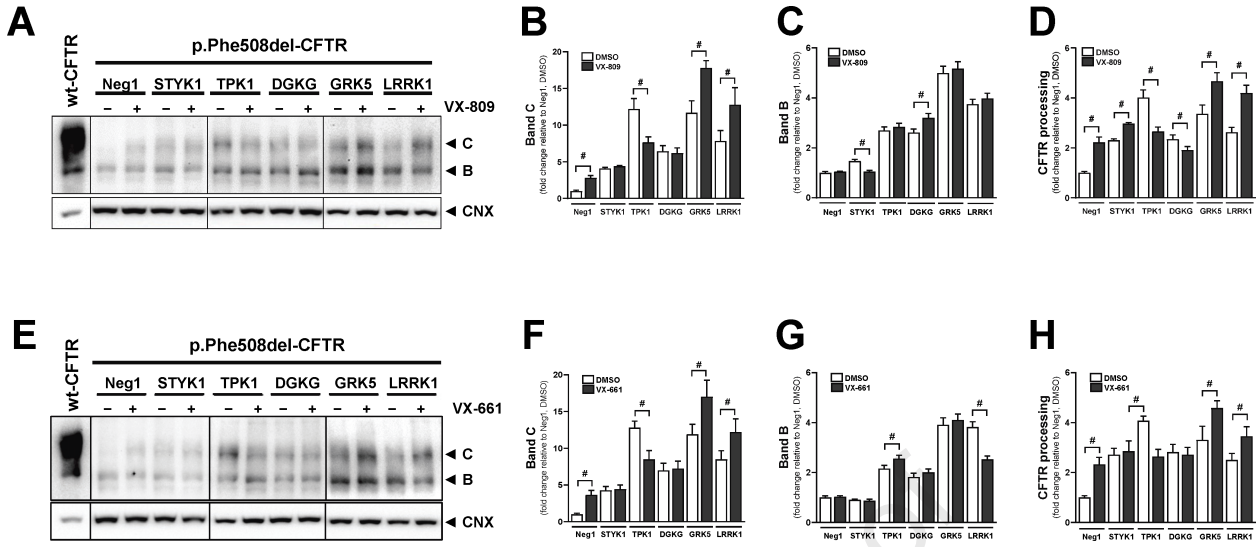

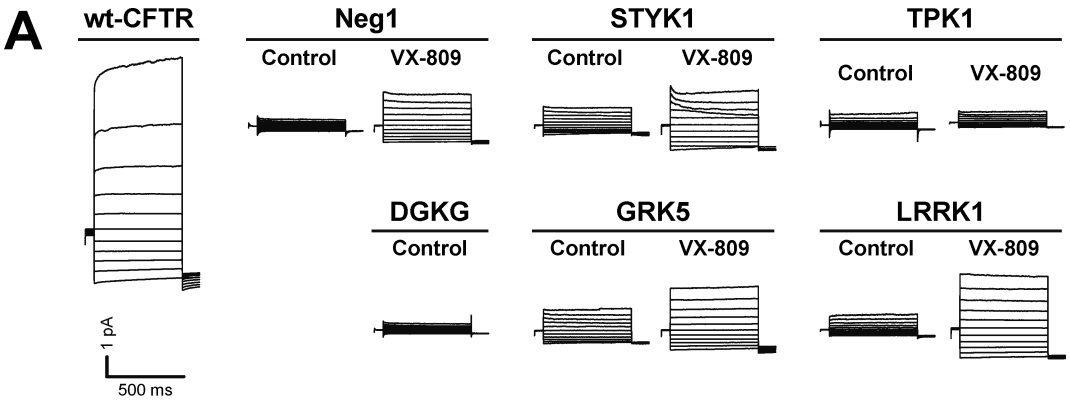

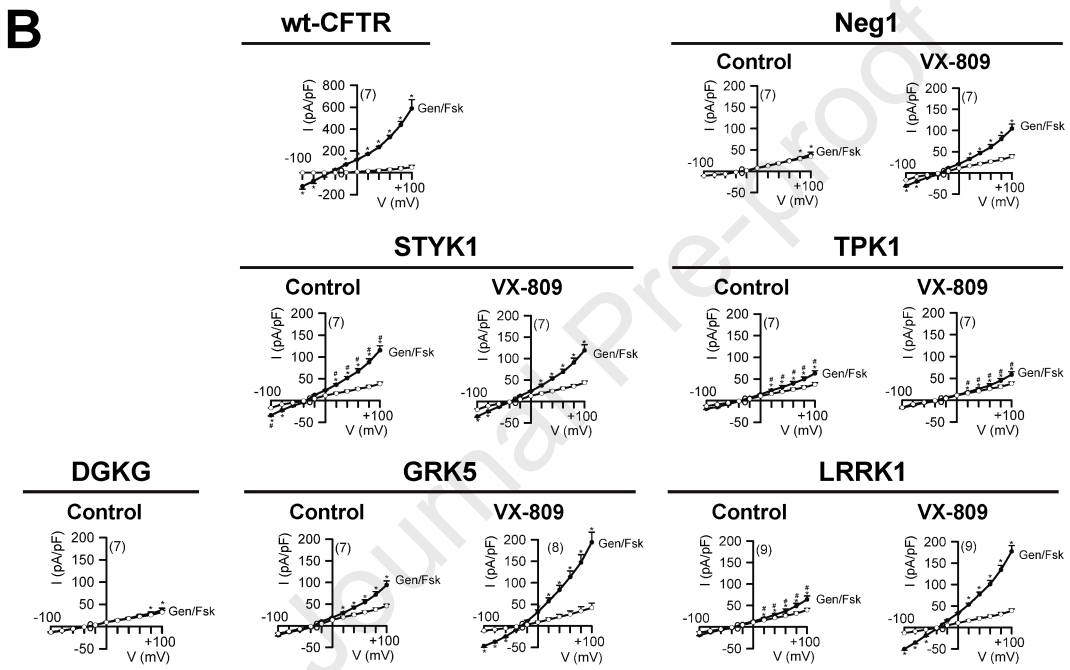

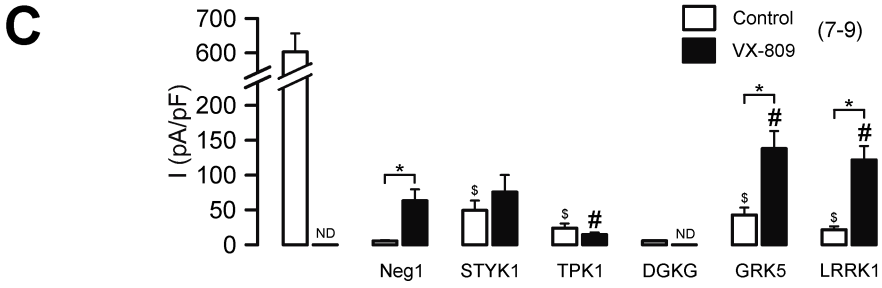

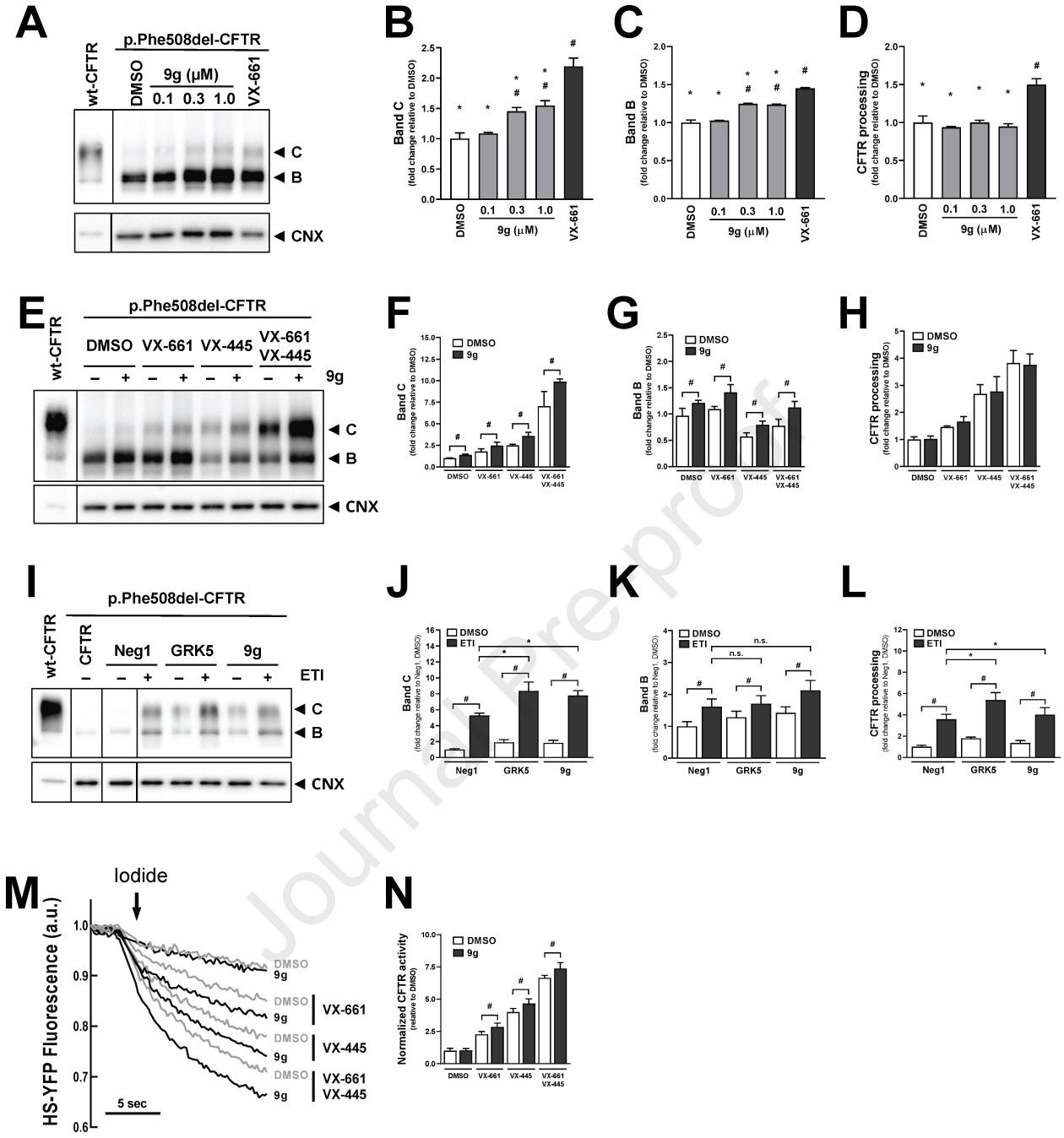

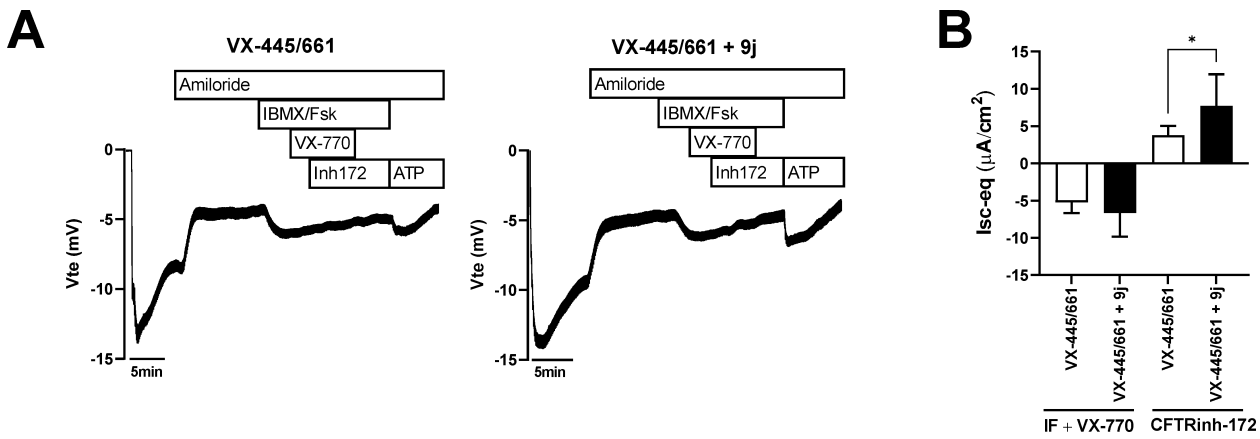

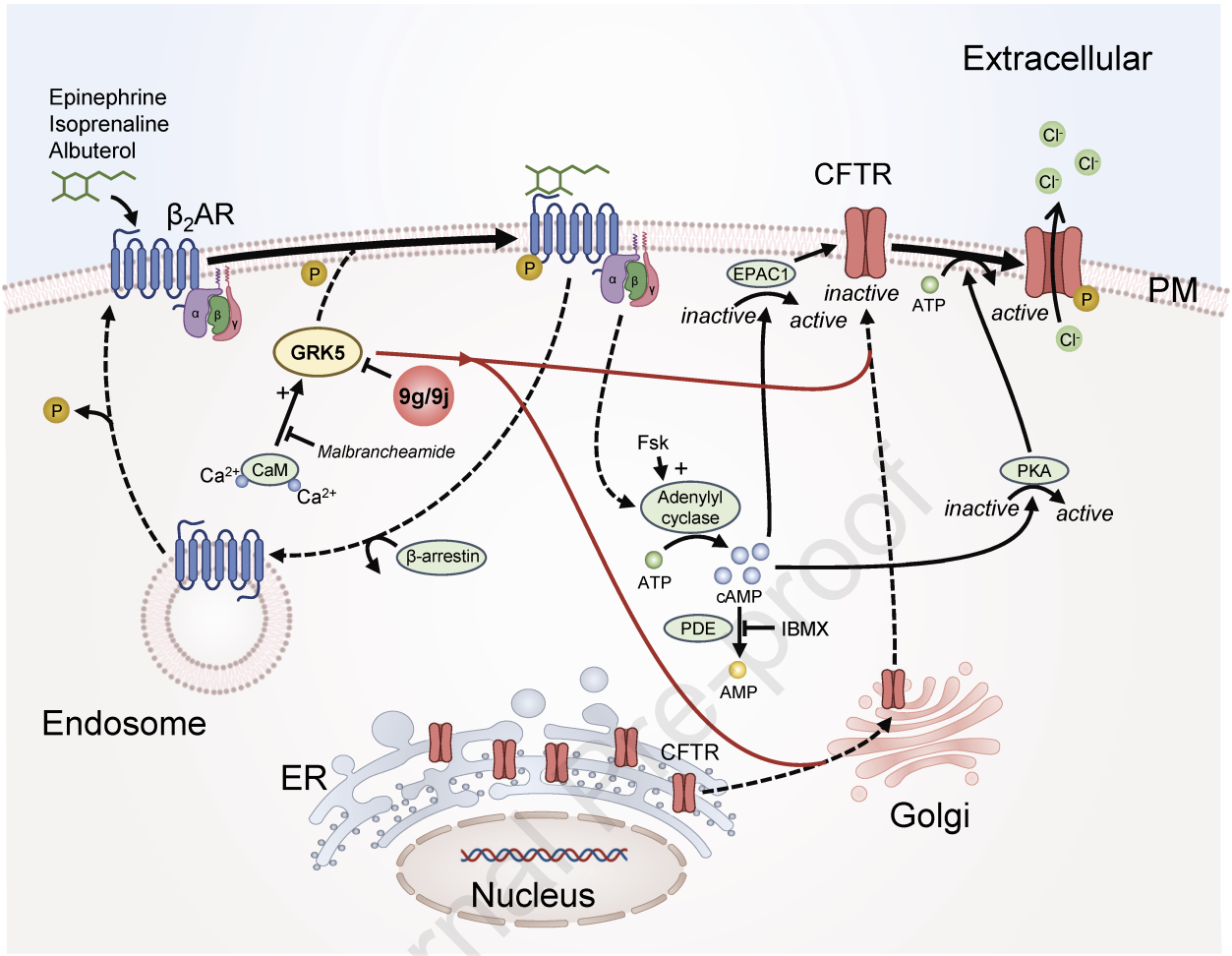

Global Functional Genomics Reveals GRK5 as a Cystic Fibrosis Therapeutic Target Synergistic with Current Modulators

Hugo M. Botelho[1], Miquéias Lopes-Pacheco[1], Madalena C. Pinto[1,2], Violeta Railean[1], Ines Pankonien[1], Mariana F. Caleiro[1], Luka A. Clarke[1], Vasco Cachatra[3], Beate Neumann[4], Christian Tischer[4,5], Cristina Moiteiro[3], Jiraporn Ousingsawat[2], Karl Kunzelmann[2], Rainer Pepperkok[4], Margarida D. Amaral[1]*

[1]BioISI – Biosystems & Integrative Sciences Institute, Faculty of Sciences, University of Lisboa. Campo Grande, 1749-016 Lisboa, Portugal

[2]Department of Physiology, University of Regensburg. Universitätsstrasse 31, 93053 Regensburg, Germany

[3]Centro de Química Estrutural, Institute of Molecular Sciences, Department of Chemistry and Biochemistry, Faculty of Sciences, University of Lisboa. Campo Grande, 1749-016 Lisboa, Portugal

[4]Cell Biology and Biophysics Unit and Advanced Light Microscopy Facility. European Molecular Biology Laboratory (EMBL). Meyerhofstraße 1, 69117 Heidelberg, Germany

[5]Centre for Bioimage Analysis. European Molecular Biology Laboratory (EMBL). Meyerhofstraße 1, 69117 Heidelberg, Germany

* Correspondence:

Email: mdamaral@ciencias.ulisboa.pt

Tel: +351 21 750 0861

Fax: +351 21 750 0088

Highlights

- Large scale high-content screen identifies p.Phe508del-CFTR traffic regulator genes
- Validation of hit genes and classification according to ERQC checkpoints
- Chemical inhibition of GRK5 rescues p.Phe508del-CFTR traffic and function
- GRK5 inhibition is additive to CFTR modulators, a potential therapeutic option

KEY RESOURCES TABLE

REAGENT or RESOURCE	SOURCE	IDENTIFIER
Antibodies		
Mouse monoclonal anti-FLAG (clone M2)	Sigma-Aldrich	Cat#F1804
Donkey anti-mouse Alexa Fluor 647	Invitrogen	Cat#A31571
Mouse monoclonal anti-CFTR	CFF Therapeutics	Cat#596
Mouse monoclonal anti-calnexin (clone 37)	BD Transduction Laboratories	Cat#610523
Bacterial and virus strains		
Biological samples		
Chemicals, peptides, and recombinant proteins		
Puromycin	Sigma-Aldrich	Cat#P8833
Blasticidin	InvivoGen	Cat#ant-bl
G418	Sigma-Aldrich	Cat#A1720
Doxycycline	Sigma-Aldrich	Cat#9891
Forskolin	Sigma-Aldrich	Cat#F6886
IBMX	Sigma-Aldrich	Cat# I5879
CFTRinh-172	MedChemExpress	Cat#HY-16671
Genistein	Sigma-Aldrich	Cat#G6649
VX-445	Selleckchem	Cat#S8851
VX-661	Selleckchem	Cat#S7059
VX-770	Selleckchem	Cat#S1144
VX-809	Selleckchem	Cat#S1565
Hoechst 33342	Sigma Aldrich	Cat#B2261
9g (CCG-273463)	This work, synthesized as in Rowlands et al. [1]	N/A
9j (CCG-273441)	MedChemExpress	Cat#HY-47573
Resazurin	Sigma-Aldrich	Cat#R7017
Critical commercial assays		
SsoFast EvaGreen	Bio-Rad	Cat#1725201
Deposited data		
Image and data analysis of the primary and secondary siRNA screens	This paper	https://doi.org/10.5281/zenodo.6617740
CFTR interactomes	This paper plus Pankow et al.[2], Canato et al.[3], Reilly et al.[4], Tomati et al.[5], Dang et al.[6], Almaça et al.[7], Simpson et al.[8]	https://doi.org/10.5281/zenodo.6646236
Experimental models: Cell lines		
CFBE41o- mCherry-Flag-wt-CFTR	Botelho et al.[9]	http://dx.doi.org/10.1038/srep09038
CFBE41o- mCherry-Flag-p.Phe508del-CFTR	Botelho et al.[9]	http://dx.doi.org/10.1038/srep09038
CFBE41o- mCherry-Flag-p.Phe508del-4RK	Canato et al.[3]	http://dx.doi.org/10.1007/s00018-018-2896-7
CFBE41o- mCherry-Flag-p.Phe508del-p.Arg1070Trp-CFTR	Canato et al.[3]	http://dx.doi.org/10.1007/s00018-018-2896-7

CFBE41o- mCherry-Flag-p.Phe508del-p.Gly550Glu-CFTR	Canato et al.[3]	http://dx.doi.org/10.1007/s00018-018-2896-7
CFBE41o- mCherry-Flag- DD/AA-CFTR	Canato et al.[3]	http://dx.doi.org/10.1007/s00018-018-2896-7
CFBE41o- YFP-H148Q/I152L wt-CFTR	Laboratory of Nicoletta Pedemonte	http://dx.doi.org/10.1152/ajpcell.00507.2010
CFBE41o- YFP-H148Q/I152L p.Phe508del-CFTR	Laboratory of Nicoletta Pedemonte	http://dx.doi.org/10.1152/ajpcell.00507.2010
CFBE41o- wt-CFTR	Laboratory of John P. Clancy	http://dx.doi.org/10.1113/jphysiol.2005.096669
CFBE41o- p.Phe508del-CFTR	Laboratory of John P. Clancy	http://dx.doi.org/10.1113/jphysiol.2005.096669
Experimental models: Organisms/strains		
Primary human bronchial epithelial cells	Laboratory of Nicoletta Pedemonte	N/A
Oligonucleotides		
Ambion Silencer Human Extended Druggable Silencer siRNA library	Ambion	N/A
Secondary and classification siRNA libraries (Silencer Select)	Ambion	This paper
siRNA (Silencer Select) Negative control Antisense (5' -> 3'): UUACGUCGUCGCGUCGUUAtt	Ambion	Cat#4390843
siRNA (Silencer Select) targeting DGKG Antisense (5' -> 3'): UUCUGUAUAUUAGUAUCUGcg	Ambion	Cat#s3918
siRNA (Silencer Select) targeting GRK5 Antisense (5' -> 3'): UUUCAGAUCUCGGUAGACGgt	Ambion	Cat#s6087
siRNA (Silencer Select) targeting LRRK1 Antisense (5' -> 3'): UCAUAUACAAUGCGAGGCCtg	Ambion	Cat#s36138
siRNA (Silencer Select) targeting STYK1 Antisense (5' -> 3'): UAGUAACCAACAAAGUUGGga	Ambion	Cat#s30824
siRNA (Silencer Select) targeting TPK1 Antisense (5' -> 3'): AAAAUAGUUGUCCAAAGGCtg	Ambion	Cat#s25692
PCR primer sequences	Harvard primerbank	https://pga.mgh.harvard.edu/primerbank
Recombinant DNA		
Software and algorithms		
CellProfiler	Carpenter et al[10]	http://cellprofiler.org
R	R Core Team	https://cran.r-project.org/
R scripts	This paper	https://doi.org/10.5281/zenodo.6617740
ImageLab	Bio-Rad	https://www.bio-rad.com/product/image-lab-software
PULSE	HEKA	N/A
Chart	AD Instruments	N/A

Panther	Laboratory of Paul D. Thomas	http://www.pantherdb.org
GraphPad Prism	GraphPad	https://www.graphpad.com/scientific-software/prism
Other		
Multidrop™ Combi	ThermoFisher	Cat#5840300
Leica DMI6000 B	Leica Microsystems	N/A
Infinite F200 Pro	Tecan	N/A
EPC 7 patch clamp amplifier	List Medical Electronics	N/A
LIH1600 interface	HEKA	N/A
Victor 3V	PerkinElmer	N/A

1. Rowlands, R.A., Chen, Q., Bouley, R.A., Avramova, L.V., Tesmer, J.J.G., and White, A.D. (2021). Generation of Highly Selective, Potent, and Covalent G Protein-Coupled Receptor Kinase 5 Inhibitors. J Med Chem *64*, 566-585. 10.1021/acs.jmedchem.0c01522.
2. Pankow, S., Bamberger, C., Calzolari, D., Martínez-Bartolomé, S., Lavallée-Adam, M., Balch, W.E., and Yates, J.R., 3rd (2015). ΔF508 CFTR interactome remodelling promotes rescue of cystic fibrosis. Nature *528*, 510-516. 10.1038/nature15729.
3. Canato, S., Santos, J.D., Carvalho, A.S., Aloria, K., Amaral, M.D., Matthiesen, R., Falcao, A.O., and Farinha, C.M. (2018). Proteomic interaction profiling reveals KIFC1 as a factor involved in early targeting of F508del-CFTR to degradation. Cell Mol Life Sci *75*, 4495-4509. 10.1007/s00018-018-2896-7.
4. Reilly, R., Mroz, M.S., Dempsey, E., Wynne, K., Keely, S.J., McKone, E.F., Hiebel, C., Behl, C., and Coppinger, J.A. (2017). Targeting the PI3K/Akt/mTOR signalling pathway in Cystic Fibrosis. Sci Rep *7*, 7642. 10.1038/s41598-017-06588-z.
5. Tomati, V., Pesce, E., Caci, E., Sondo, E., Scudieri, P., Marini, M., Amato, F., Castaldo, G., Ravazzolo, R., Galietta, L.J.V., and Pedemonte, N. (2018). High-throughput screening identifies FAU protein as a regulator of mutant cystic fibrosis transmembrane conductance regulator channel. J Biol Chem *293*, 1203-1217. 10.1074/jbc.M117.816595.
6. Dang, H., Polineni, D., Pace, R.G., Stonebraker, J.R., Corvol, H., Cutting, G.R., Drumm, M.L., Strug, L.J., O'Neal, W.K., and Knowles, M.R. (2020). Mining GWAS and eQTL data for CF lung disease modifiers by gene expression imputation. PLoS One *15*, e0239189. 10.1371/journal.pone.0239189.
7. Almaça, J., Faria, D., Sousa, M., Uliyakina, I., Conrad, C., Sirianant, L., Clarke, L.A., Martins, J.P., Santos, M., Hériché, J.-K., et al. (2013). High-content siRNA screen reveals global ENaC regulators and potential cystic fibrosis therapy targets. Cell *154*, 1390-1400. 10.1016/j.cell.2013.08.045.
8. Simpson, J.C., Joggerst, B., Laketa, V., Verissimo, F., Cetin, C., Erfle, H., Bexiga, M.G., Singan, V.R., Heriche, J.K., Neumann, B., et al. (2012). Genome-wide RNAi screening identifies human proteins with a regulatory function in the early secretory pathway. Nat Cell Biol *14*, 764-774. 10.1038/ncb2510.
9. Botelho, H.M., Uliyakina, I., Awatade, N.T., Proenca, M.C., Tischer, C., Sirianant, L., Kunzelmann, K., Pepperkok, R., and Amaral, M.D. (2015). Protein traffic disorders: an effective high-throughput fluorescence microscopy pipeline for drug discovery. Sci Rep *5*, 9038. 10.1038/srep09038.
10. Carpenter, A.E., Jones, T.R., Lamprecht, M.R., Clarke, C., Kang, I.H., Friman, O., Guertin, D.A., Chang, J.H., Lindquist, R.A., Moffat, J., et al. (2006). CellProfiler: image analysis software for identifying and quantifying cell phenotypes. Genome Biol *7*, R100. 10.1186/gb-2006-7-10-r100.